A butterfly pan-genome reveals that a large amount of structural variation underlies the evolution of chromatin accessibility

Authors

Angelo A. Ruggieri[1], Luca Livraghi[2,3], James J. Lewis[4], Elizabeth Evans[1], Francesco Cicconardi[5], Laura Hebberecht[5], Yadira Ortiz-Ruiz[1,6], Stephen H. Montgomery[5], Alfredo Ghezzi[1], José Arcadio Rodriguez-Martinez[1], Chris D. Jiggins[7], W. Owen McMillan[3], Brian A. Counterman[8], Riccardo Papa[1,6] & Steven M. Van Belleghem[1,9]

Affiliations

[1]Department of Biology, University of Puerto Rico, Rio Piedras, Puerto Rico.
[2]Department of Biological Sciences, The George Washington University, Washington DC, USA.
[3]Smithsonian Tropical Research Institute, Republic of Panama.
[4]Department of Zoology, University of British Columbia, Vancouver, BC, Canada.
[5]School of Biological Sciences, Bristol University, UK.
[6]Molecular Sciences and Research Center, University of Puerto Rico, San Juan, PR.
[7]Department of Zoology, University of Cambridge, Cambridge, UK.
[8]Department of Biological Sciences, Auburn University, Auburn, Alabama, USA.
[9]Ecology, Evolution and Conservation Biology, Biology Department, KU Leuven, Leuven, Belgium.

Abstract

Despite insertions and deletions being the most common structural variants (SVs) found across genomes, not much is known about how much these SVs vary within populations and between closely related species, nor their significance in evolution. To address these questions, we characterized the evolution of indel SVs using genome assemblies of three closely related *Heliconius* butterfly species. Over the relatively short evolutionary timescales investigated, up to 18.0% of the genome was composed of indels between two haplotypes of an individual *H. charithonia* butterfly and up to 62.7% included lineage-specific SVs between the genomes of the most distant species (11 Mya). Lineage-specific sequences were mostly characterized as transposable elements (TEs) inserted at random throughout the genome and their overall distribution was similarly affected by linked selection as single nucleotide substitutions. Using chromatin accessibility profiles (i.e., ATAC-seq) of head tissue in caterpillars to identify sequences with potential *cis*-regulatory function, we found that out of the 31,066 identified differences in chromatin accessibility between species, 30.4% were within lineage-specific SVs and 9.4% were characterized as TE insertions. These TE insertions were localized closer to gene transcription start sites than expected at random and were enriched for sites with significant resemblance to several transcription factor binding sites with known function in neuron development in *Drosophila*. We also identified 24 TE insertions with head-specific chromatin accessibility. Our results show high rates of structural genome evolution that were previously overlooked in comparative genomic studies and suggest a high potential for structural variation to serve as raw material for adaptive evolution.

Running title

Functional potential of structural variants

Keywords

Heliconius butterflies, structural variation, indels, pan-genome, transposable elements, chromatin accessibility, ATAC-seq

Introduction

Structural variants (SVs) in genomes are a ubiquitous component of within and between species genomic variation (Zhang et al. 2021; Mérot et al. 2020). The larger size of SVs, when compared to single nucleotide polymorphisms (SNPs), may increase their likelihood of being involved in maladaptation (Collins et al. 2020). However, there are a growing number of examples of an important role of SVs in adaptive innovations (Lucek et al. 2019; Wellenreuther et al. 2019). For example, increased linkage disequilibrium and recombination suppression within large inversions can initiate co-adaptation of gene complexes in the re-arranged genomic haplotype (e.g., supergenes; Jay et al. 2021; Matschiner et al. 2022). Alternatively, insertion-deletion mutations (indels) can include one or multiple functional genetic elements and studies are starting to indicate that genomic indel content might be large relative to the more commonly studied Single Nucleotide Polymorphisms (SNPs). A study of humans found 2.3 million indels of 1 to 49 bp in length and 107,590 indels larger than 50 bp that accounted for up to 279 Mb in sequence differences among individuals (Ebert et al. 2021). Several studies in plants and fungi identified the widespread presence of SVs, often linked to phenotypic variation (Plissonneau et al. 2018; Read et al. 2013; Hübner et al. 2019). Aside from these studies carried out on humans and non-metazoans, a few studies in mollusks have also unveiled the possibility that gene-carrying indels may be much more widespread than originally thought (Calcino et al. 2021; Gerdol et al. 2020). Another case are *Oedothorax* dwarf spiders, in which a large 3 Mb indel is associated with an elaborate alternative reproductive male morph (Hendrickx et al. 2022).

A major challenge in studying the relationships between SVs and adaptive diversification has been the difficulty in characterizing the landscape of divergence in repetitive and rearranged regions of genomes. To overcome this, we here used high-quality butterfly genomes of three *Heliconius* species common to Central and South America and constructed a pan-genome alignment that allowed us to quantify the homologous and non-homologous (i.e., lineage-specific insertions or deletions) portions of their genomes. *Heliconius charithonia* is about 11.1 (8.8-13.4) MY divergent from *H. melpomene* and 6.0 (4.8-7.4) MY divergent from *H. erato* (Kozak et al. 2015; Cicconardi et al. 2022) (Fig. 1A). The three species are reproductively isolated and differ in host plant use (Brown 1981; Jiggins 2017), larval gregariousness (Beltrán et al. 2007), flight (Mallet and Gilbert 1995), pupal mating rates (Thurman et al. 2018; Mendoza-Cuenca and MacÍas-Ordóñez 2010), and brain structure (Montgomery and Merrill 2017).

With the pan-genome alignment, we first analyzed the frequency, length distribution, and composition of lineage-specific sequences between the species. Second, we studied the evolutionary processes affecting the distribution and frequency of SVs. We expected that if SVs have a higher chance of being maladaptive, we will see a lower abundance of SVs on smaller chromosomes compared to SNPs. This expectation is derived from smaller chromosomes having a higher per base pair recombination rate that could lead them to purge maladaptive SVs more efficiently (Hill and Robertson 1966). In contrast, if SVs have a similar maladaptive load as SNPs, we expect their abundance on chromosomes to be similar to SNPs, which have a higher abundance on smaller compared to larger chromosomes in *Heliconius* resulting from the higher recombination rate and thus lower reduction of SNP diversity by linked selection on smaller chromosomes (Cicconardi et al. 2021; Martin et al. 2019). To further understand the maladaptive impact of SVs, we also characterized the distribution of SVs relative to gene density. Our hypothesis is that if intergenic SVs impact gene functioning negatively, then we expected to identify fewer SVs in gene rich regions. Moreover, if SVs negatively impact gene regulation, we expect their distances from the transcription start sites (TSS) of genes to be further compared to a random sample of genome positions.

Third, in contrast to maladaptive impacts of SVs, differences in the presence and/or accessibility of *cis*-regulatory loci (i.e., non-coding functional regions of the genome that influence patterns of gene expression) between divergent populations have been shown to be responsible for adaptive differences within and between species of *Heliconius* butterflies (Lewis et al. 2020, 2019; Livraghi et al. 2021). Therefore, to investigate the functional significance of intergenic SVs, we annotated our pan-genome with assays of chromatin accessibility, a powerful approach to identify active *cis*-regulatory sequences (Buenrostro et al. 2013). We focused on chromatin profiles of developing head tissue and wings as a control and observed that lineage-specific open chromatin is substantially associated with SVs. To investigate whether these lineage-specific open chromatin regions within SVs have been involved in recent adaptive evolution, we used selective sweep scans. We also correlated their abundance with gene density and TSS and compared this correlation to that of SVs that do not associate with lineage-specific changes in chromatin accessibility. Finally, using motif enrichment scans for sites with significant similarity to *Drosophila* transcription factor (TF) binding sites, we investigated whether these lineage-specific SVs carry a high potential for structural variation to serve as material for adaption. In summary, our work here provides a uniquely comprehensive test for the role of SVs in adaptive evolution.

Results

Genome assemblies, pan-genome alignment, and lineage-specific sequence composition

We *de novo* sequenced and assembled two haploid genomes from a single *H. charithonia* individual from Puerto Rico using 10x chromium technology (10x Genomics, San Francisco, USA). The two pseudo-haploid *H. charithonia* genomes had a length of 355.2 Mb and 361.5 Mb. For *H. erato* and *H. melpomene* we used previously published reference genomes from individuals from Panama which had assembly lengths of 382.8 Mb and 275.2 Mb, respectively (Van Belleghem et al. 2017; Davey et al. 2016). All assemblies had a BUSCO completeness higher than 98.9% (Supplemental Table S1).

Effective population size influences genetic diversity in SNPs (Charlesworth 2009; Leffler et al. 2012) and is thus also likely to be a major influence on indel diversity. We therefore reconstructed the historical population sizes from diversity estimates in whole-genome resequenced samples using PSMC (pairwise sequentially Markovian coalescent). These reconstructions suggest that populations from Panama have had an increase in population size over the past one MY, with *H. erato* and *H. charithonia* having a larger population size than *H. melpomene* over the last 300 ky (Fig. 1B). In contrast, two *H. charithonia* individuals from Puerto Rico suggest a population size decline over the past 200 Kya.

For this study, we aligned the four genomes (two *H. charithonia* pseudo-haplotypes, *H. erato* and *H. melpomene*) into a pan-genome with a total length of 659.4 Mb. Among the three species, only 138.6 Mb (21.0%) of sequence was identified as homologous. However, this conserved sequence part retained a high BUSCO completeness of 94.9%, demonstrating it contains the highly conserved gene coding fraction of the genome (Supplemental Table S1). When investigating the proportions of non-homologous (lineage-specific) sequences as obtained from the pan-genome, we found that the lineage-specific sequence proportion increases with phylogenetic distance (Fig. 1C). More divergent phylogenetic comparisons also had lineage-specific sequences that were generally longer (Fig. 1D), whereas less divergent phylogenetic comparisons had a higher proportion of lineage-specific sequences being accounted for by single base pair insertions (e.g., 25.7% of lineage-specific sequence between the *H. charithonia* haplotypes versus 5.8% of lineage-specific sequences between *H. charithonia* and *H. erato*;

Supplemental Table S2). Between the *H. charithonia* pseudo-haplotypes we observed two genes within an indel, a endonuclease-reverse transcriptase related to a TE (evm.TU.Herato1801.176) and a zinc finger DNA-binding protein (evm.TU.Herato1104.1). Sequences specific to *H. erato* included 167 genes that were absent in the *H. charithonia* genome, and 317 genes absent in the *H. melpomene* genome (Supplemental Table S3). Of these, only two genes that were absent in *H. charithonia* were present in *H. melpomene*, which suggests that almost all genes unique to *H. erato* resulted from gene gain rather than loss in the other species. Of the lineage-specific genes, 22.3% were related to TEs, 4 genes were characterized to have a function in repressing TE activity and 10 genes were zinc finger proteins for which some families are involved in TE repressing (Ecco et al. 2017). Additionally, 7 genes were involved in neural activity, 4 genes were involved in chemosensing and 33.6% were uncharacterized. In the different genome comparisons, we could further determine the identity of 43.9 to 82.0% of all the lineage-specific sequences, with TE insertions being the most abundant SVs (Supplemental Table S2).

Among phylogenetic comparisons, we found generally similar patterns of TE family accumulation but observed several lineage-specific differences (Fig. 2). The most abundant elements associated with lineage-specific sequences in all genome comparisons were *SINE* elements (25 to 41%), *Rolling-circle* elements (23 to 35%), *LINE* elements (10.1 to 22.4%), and *DNA transposable* elements (14.8 and 21.25%) (Fig. 2A). Our phylogenetic framework next allowed us to characterize the time of accumulation for TEs along the *H. erato/H. charithonia* branch (considering *H. melpomene* as the outgroup). Within the TE families, we found that *Metulj-7* elements accumulated before *H. erato* and *H. charithonia* split (Fig. 2B). This was also supported by relative age of accumulation analysis based on divergence of *Metulj-7_Hmel* that showed accumulation was more ancient than, for example, *Metulj_m51* that likely increased in number after *H. charithonia* and *H. erato* split (Supplemental Fig. S1A). *Metulj-7_Hmel* also accrued earlier in the *H. melpomene* lineage (Supplemental Fig. S1B). This implies an accumulation that preceded the split of our butterfly lineages. The reduction of *Metulj-7_Hmel* in more recent times supports a similar finding by Ray *et al.* (2019), who observed a reduction of *Metulj-7_Hmel* accumulation in the *H. charithonia/erato* lineage starting at 5 Mya (Ray et al 2019). Between the two *H. charithonia* haplotypes, the two most abundant groups associated with indels were *Rolling-circle* (32.5%) and *SINE* (29.7%), with *Helitron2_Hera* and *Metulj7_Hmel* showing highest copy numbers (6.5 and 3.6% variation in activity, respectively; Fig. 2C). As higher copy numbers of *Helitron2_Hera* were not observed along any other parts of the phylogeny, this suggests that *Helitron2_Hera* accumulated more recently, causing indels. In contrast, the high copy numbers of *Metulj-7_Hmel* in indels indicates that these indels may persist over long time scales.

Indel patterns and chromosome sizes

Between the homologous fraction of the genomes (i.e., subtracting lineage-specific sequence from the genome length), we calculated that the frequency of SVs between the two pseudo-haplotypes of the *H. charithonia* individual was 0.010 per bp and slightly higher than the SNP frequency of 0.007 per bp between these haplotypes. Single bp indels were most frequent and SVs shorter than 50 bp accounted for 98.1% of all indels in *H. charithonia* (Supplemental Table S2). In contrast, when comparing species, substitutions were 3.7 to 3.8 times more frequent than SVs, with 0.030 SVs per bp versus 0.110 substitutions per bp between *H. charithonia* and *H. erato* and 0.039 SVs per bp versus 0.148 substitutions per bp between *H. charithonia* and *H. melpomene* (Fig. 3). This change in relative frequencies of SNPs

and SVs could be largely ascribed to more single bp indels between the pseudo-haplotypes of *H. charithonia* compared to interspecies comparisons (Fig. 1D; Supplemental Table S2).

We next examined if the abundance of SVs across the genome is similarly affected by linked selection as SNP diversity. In *Heliconius*, there is a negative relationship between average nucleotide diversity (i.e., average pairwise nucleotide differences) and chromosome size, with larger chromosomes generally carrying lower diversity (Fig. 3A; Martin et al. 2019; Cicconardi et al. 2021). In the case of nucleotide diversity and chromosome size, this negative relationship has been explained by an increased reduction of genetic diversity at linked sites by greater background selection and genetic hitchhiking on larger chromosomes (Cicconardi et al. 2021; Campos and Charlesworth 2019; Cutter and Payseur 2013). Genetic linkage maps suggest that there is on average a single crossover per meiosis, regardless of chromosomal length (Davey et al., 2016). This results in longer chromosomes having a lower per-base recombination rate, which increases the extent of linked selection and results in lower nucleotide diversity on larger chromosomes. However, if SVs have a higher maladaptive mutation load because of their size, we might expect the opposite pattern in which shorter chromosomes with higher recombination rates were able to purge SVs more easily through recombination (Hill and Robertson 1966). Thus, there might be a positive relationship between SV frequency and chromosome length. Our data are most consistent with the hypothesis that SVs are affected by linked selection in a manner similar to SNPs. Indeed, between the two pseudo-haplotypes of *H. charithonia*, there was a significant negative relationship between the indel frequency in each chromosome and chromosome sizes (Fig. 3C). This suggests that the general SV frequency in a population may be driven by linked selection similar to SNPs. Patterns of the frequency of lineage-specific sequences may then have been largely driven by patterns of ancestral diversity, resulting in higher frequencies of lineage-specific sequences on smaller chromosomes (Fig. 3D-F), as is also observed for pairwise nucleotide divergence patterns between, for example, *H. charithonia* and *H. erato* and *H. melpomene* (Fig. 3B; Van Belleghem et al. 2018). This relationship between SV frequency and chromosome length holds for SVs of different size classes (1 bp indels, 2-50 bp, and >1,000 bp; Supplemental Fig. S2).

The expectation of linked selection similarly affecting SNPs and SVs is further borne out on the sex (Z) Chromosome (21), where there was a reduction in SV frequency that roughly mirrored the patterns of SNP diversity. Due to its hemizygous state in females, there is a smaller effective population size (0.75 relative to autosomes) and an expected reduction in SNP diversity (Charlesworth 2001). For indels within *H. charithonia*, we found a 0.77 ratio of indel frequency on Chromosome 21 compared to the autosomes, suggesting that indels are subject to differences in effective population size similarly to SNPs.

We next characterized the distribution of SVs relative to genes to further explore the potential maladaptive impact of SVs. TEs, the most abundant SVs, are argued to most often have a neutral or negative impact and end up silenced by genome defense mechanisms (Okamoto and Hirochika 2001; Rigal and Mathieu 2011). If intergenic TEs impact gene functioning negatively, we expected to identify fewer TEs in gene rich regions. Moreover, if TEs negatively impact gene regulation, we expected their distances from the 5'-end of genes (as a proxy for the transcription start site (TSS)) to be further compared to a random sample of genome positions. In agreement with the former expectation, the frequency of lineage-specific TEs correlated negatively with gene frequency (R^2 = -0.27, $p < 0.001$; Fig. 4A), suggesting a general purifying selection against SVs and TEs in gene dense regions. The distance distribution of TEs to TSS was significantly higher than random expectations although visually similar

(Fig. 4B), which may reflect their tendency to randomly insert in the genome in terms of genomic position.

Genomic landscape of DNA accessibility and functional potential of TEs

Although the genome-wide distribution patterns of SVs and TEs seems to be affected by linked selection, we next wanted to investigate the functional and adaptive significance of lineage-specific intergenic SVs. TEs, for example, have been suggested to be important genomic material for *cis*-regulatory element evolution (Branco and Chuong 2020; Pontis et al. 2019; Fueyo et al. 2022). To test this, we studied the genomic distribution of potential *cis*-regulatory elements (CREs) using Assays for Transposase-Accessible Chromatin using sequencing (ATAC-seq) (Buenrostro et al. 2013). We obtained ATAC-seq data for head tissue from 5th instar caterpillars, a tissue labile to adaptive change (Montgomery and Merrill 2017; Montgomery et al. 2021) and a developmental stage that can be confidently timed (Reed et al. 2007) to minimize differences in developmental rates between species that could otherwise also cause differences in ATAC-seq profiles. In *H. melpomene*, *H. erato* and *H. charithonia*, we counted, respectively, 21,708, 28,264 and 21,097 ATAC-seq peaks that significantly represented open chromatin (Fig. 4C). Of these peaks, 6,611 (13.8%) of the total recorded peaks were identified as homologous (overlapped at least 50% reciprocally between all three species), whereas 31,066 were lineage-specific. Although some of the lineage-specific chromatin accessible peaks may result from differences in developmental timing between the three species and some signals may not have reached ATAC-seq peak calling thresholds in one of the species (i.e., false negatives), we find that out of these 31,066 lineage-specific peaks, 9,456 (30.4%) were within SVs of which 2,915 (9.4%) could be annotated as TEs.

If open chromatin indeed correlates with active gene regulation, we expected to find more ATAC-seq peaks in gene dense regions of the genome. In agreement with such active gene regulation, ATAC-seq peaks were indeed enriched in regions of the genome with higher gene density ($R^2 = 0.23$, $p < 0.001$; Fig. 4D). This positive correlation with gene density was also observed for ATAC-seq peaks that were lineage-specific ($R^2 = 0.36$, $p < 0.001$), and ATAC-seq peaks that were within lineage-specific SVs and TEs ($R^2 = 0.22$, $p < 0.001$), which supports that they may also have *cis*-regulatory activity. Moreover, these ATAC-seq peaks were closer to TSS than random and 180 were within 500 bp from a gene's TSS (Fig. 4E; Supplemental Table S4).

We next investigated if the distribution of lineage-specific ATAC-seq peaks within TEs closer to TSS may have been caused by inserting in open chromatin, or whether these TE insertions may have caused the open chromatin and have been selectively retained at these positions. For this, we need to consider that the ATAC-seq peaks identified in the head tissue could also be accessible in the germline where TE insertions must occur to be heritable. We looked for chromatin signals in homologous sequences flanking the TEs in the other species and found that 395 (13.5%) out of 2,915 lineage-specific TEs with ATAC-seq peaks had a significant ATAC-seq signal in the other species within 2,000 bp of homologous sequence flanking the insert. This was higher than an expected 2% obtained from 1,000 random permutations of an equal number of TEs that did not associate with ATAC-seq peaks. Nevertheless, 2,520 (86.4%) did not have any ATAC-seq signal in the other species. To further test whether these TEs have been selectively retained closer to TSS, we performed a TSS distance distribution comparison of SVs within ATAC-seq peaks specific to *H. charithonia* (Fig. 4F). A comparison relative to *H. erato* and *H. melpomene* showed

significantly closer TSS distances of lineage-specific sequences with ATAC-seq peaks compared to random (Wilcoxon p-value < 0.001), whereas the distribution of indels with ATAC-seq peaks within the single *H. charithonia* individual was not statistically different compared to a random distribution of positions in the genome (Wilcoxon p-value = 0.18).

Although the distribution of ATAC-seq peaks within TEs can fit selective retention of these SVs, we wanted to directly test for the influence of selection using selective sweep analysis. Given the demographic history of our taxa and using an effective population size of 2 million individuals (Moest et al. 2020), it is important to recognize that our ability to identify signals of adaptation is restricted to selection acting within the past 80,000 years (0.6% of the studied evolutionary timescale). Under these restricted conditions, we did not find a pattern of recent adaptive evolution (Supplemental Fig. S3). We did observe that TE insertions associated with open chromatin were more fragmented compared to other TEs in the genome (Supplemental Fig. S4).

In several studies, TEs have been correlated to evolutionary changes in chromatin state, gene expression, and adaptive evolution at a genome-wide scale (Bourque et al. 2018; Diehl et al. 2020; Ohtani and Iwasaki 2021; Liu et al. 2019). The TE family composition of TEs that associated with open ATAC-seq peaks was markedly different between the three *Heliconius* species (Supplemental Fig. S5). To infer the evolutionary potential of the accumulated TE families, we next identified enrichment of sequence motifs in ATAC-seq peaks that are within lineage-specific TE insertions and investigated their potential as transcription factor (TF) binding sites. TF binding motif enrichment analysis on the 2,915 lineage-specific ATAC-seq peaks within TE insertions showed that each genome has unique signals of binding site enrichment with significant similarity to binding sites of TFs in *Drosophila* (Supplemental Fig. S6). Moreover, nine of the identified 21 enriched binding motifs resembled binding sites of TFs with known functions in nervous system development in *Drosophila* (Supplemental Fig. S6).

Finally, by comparing the head ATAC-seq data to that of developing wing tissue, we looked for head-specific chromatin changes within lineage-specific TE insertions. The tissue-specific accessibility of these TE insertions would provide indications that these SVs interact with tissue-specific factors and could provide strong candidates as targets of adaptive evolution. We identified 24 head-specific ATAC-seq peaks within a lineage-specific TE insertion that were not accessible in wing tissues (Fig. 5; Supplemental Table S5). Of these, 2, 4 and 18 were specific to *H. charithonia*, *H. erato* and *H. melpomene*, respectively. Five were located less than 50 kb from genes with known functions in nervous system development in *Drosophila*. In *H. melpomene*, this included the gene *sloppy paired 2* (*slp2*) that also showed TF binding site enrichment in lineage-specific ATAC-seq peaks within a TE (Supplemental Fig. S6).

Discussion

In *Heliconius*, the extent of SV within and between species has been previously limited to studies of the repetitive sequence content within individual reference genomes (Lavoie et al. 2013; Ray et al. 2019), co-linearity of genomes (Davey et al. 2017; Cicconardi et al. 2021), structural rearrangements in a 'supergene' related to a color pattern polymorphism (Joron et al. 2011; Edelman et al. 2019), and duplications that likely underestimated the extent of SV due to stringent confidence cutoffs needed when using short-read sequences (Pinharanda et al. 2017). Our approach combined four high-quality *Heliconius*

genome assemblies, including two pseudo-haplotypes, with a pan-genome alignment to quantify the extensive uniqueness between these genomes due to SVs. For example, genome wide nucleotide diversity (π) obtained from SNPs was 0.007 within *H. charithonia* and D_{XY} (average pairwise nucleotide differences) ranged from 0.11 between *H. charithonia* and *H. erato* to 0.15 between *H. charithonia* and *H. melpomene*. This suggests an average sequence divergence of 0.7% between the haplotypes of *H. charithonia* and 11 to 15% of sequence divergence between homologous parts of the genomes of these species. In contrast, SV analysis demonstrated that an additional 18.0% of the genome of *H. charithonia* included hemizygous indel sequences and up to 43.5% and 62.7% of additional genomic differences between *H. charithonia* and *H. erato* and *H. melpomene*, respectively, resulted from SVs.

In contrast to *Heliconius* populations from Panama, we observed a population size decline over the past 200 ky for *H. charithonia* from Puerto Rico, which fits with divergence time estimates from mtDNA of the Puerto Rican population (Davies and Bermingham 2002). This implies that the indel diversity as estimated from the pseudo-haplotypes of the single Puerto Rican *H. charithonia* individual in this study may be a general underestimate of indel proportions in other species or populations such as those from Panama. These populations may thus carry a high genomic fraction that is subject to presence/absence variation. While the total SV and SNP frequencies (estimated per bp) were similar between the *H. charithonia* pseudo-haplotypes, substitutions were 3.7 to 3.8 times more frequent than SVs when comparing species. Notably, this change in relative frequencies of SNPs and SVs could be largely ascribed to more single bp indels between the pseudo-haplotypes of *H. charithonia* compared to interspecies comparisons and may indicate that as the length distribution of SVs shifts to larger sizes in interspecies comparisons, negative selection against SVs may become stronger compared to SNPs. Despite this marked difference in frequencies, linked selection seems to similarly affect SNPs and SVs, indicating that most SVs are similarly affected by genetic drift and that many may be selectively neutral.

Next, using ATAC-seq data, we assessed the extent to which differences in chromatin accessibility resulted from SVs and TE insertions. We observed that out of the 515,884 SVs identified as lineage-specific TE insertions, only 0.56% were associated with changes in chromatin accessibility between species. However, out of the 31,066 identified lineage-specific changes in chromatin accessibility, 30.4% were within SVs and 9.4% were characterized as lineage-specific TEs. We also note that the absolute number of functional elements within SVs and TEs may be much higher than what is described in our study because we restricted our chromatin data to only one tissue type and developmental time point. As a comparison, a genomic study across 20 mammalian genomes spanning 180 MY of evolution identified roughly half of all active liver enhancers specific to each species, but argued that most of these lineage-specific enhancers evolved through redeployment of ancestral DNA and that a significant contribution of repeat elements to enhancer evolution was only found for more recently evolved enhancers less than 40 MY old (Villar et al. 2015).

While we did not find any indication of recent adaptive evolution using a selective sweep analysis, our observations indicate an important potential role of TEs in generating genetic variation with functional effects through changes in chromatin state and potentially the regulation of nearby genes. First, even if SVs are mostly neutral or deleterious, their shear abundance and association with chromatin accessibility differences between species underscores their adaptive potential. Second, we observed a pattern in which TE insertions associated with open chromatin were closer to TSS only in interspecies comparisons, not among the *H. charithonia* haplotypes. This pattern could have potentially arisen over time if TE insertions

closer to TSS have a higher chance of affecting gene expression and being involved in adaptive changes between species. Third, we observed that TE insertions associated with open chromatin were more fragmented compared to other TEs in the genome, which may suggest stronger selection for immobilization or adaptive change of these TE insertions (Joly-Lopez and Bureau 2018). Fourth, lineage-specific TEs that underlie changes in chromatin accessibility included 21 enriched motifs with significant similarity to *Drosophila* TF binding sites. These included *lola, Dref, shn, Hr51, slp2, wor, esg, Btd,* and *Fer1* with functions in neural development (Iyer et al. 2013; Kozlov et al. 2017; Sato and Tomlinson 2007; Ashraf et al. 2004, 1999; Wimmer et al. 2010; Guo et al. 2019). Three other TF motifs have been previously linked to wing or color pattern development in lepidoptera. *Mad* is a TF linked to wing development in *H. melpomene* (Baxter et al. 2010). *Mitf* has been associated with color pattern development in other animals (Mallarino et al. 2016; Poelstra et al. 2015), and in *Heliconius* butterflies potentially interacts with *aristaless* (Westerman et al. 2018). Finally, *dsx* controls sex-limited mimicry patterns in *Papilio polytes* and *Zerene cesonia* butterflies (Rodriguez-Caro et al. 2021; Nishikawa et al. 2015). Moreover, 24 TE insertions had head-specific accessibility compared to wing tissues and provide strong candidates as targets of adaptive evolution.

In conclusion, our comparative genome-wide quantification strategy for SVs demonstrated they can underly more than tenfold sequence differences compared to SNPs between two haploid genomes of a single individual. Such remarkable differences in genome content are also becoming more obvious in other comparative genome studies that incorporated SVs in their analysis, including comparisons between humans and chimpanzee for which genome similarity is much lower than the 99% estimated from the first comparative genomic studies that only considered SNPs and small indels (The Chimpanzee Sequencing and Analysis Consortium 2005; Suntsova and Buzdin 2020). Similar to many other organisms, the biggest proportion of these genomic differences is mainly explained by TE accumulation, (Garcia-Perez et al. 2016; Cerbin and Jiang 2018). Moreover, examples are accumulating of SVs and, in particular, TE insertions as the mutational changes underlying adaptive phenotypic variation (Schrader and Schmitz 2019). For example, in the bird genus *Corvus*, adaptive evolution of plumage patterning, a pre-mating isolation trait, was found to be the result of a TE insertion that reduced the expression of the *NDP* gene (Weissensteiner et al. 2020). Several examples also come from the genomes of Lepidoptera. In the classic example of industrial melanism of the peppered moth, a novel 21 kb TE insertion that impacts the function of the gene *cortex* is responsible for the development of the different color morphs (Van't Hof 2016). Another TE insertion has been linked to the silencing of a *cortex* regulatory region and may be responsible for the yellow band on the hindwing in geographic variants of *Heliconius melpomene* butterflies (Livraghi et al. 2021). In *Colias* butterflies, an alternative life history strategy that involves resource allocation to reproductive and somatic development and wing color polymorphism was mapped to a TE insertion near the homeobox transcription factor gene *BarH-1* (Woronik et al. 2019). In a pair of *Papilio* species, a female-limited mimetic polymorphism has been linked to a supergene including *doublesex* (*dsx*) and recombination suppression in this supergene has been suggested to result from TE accumulation (Iijima et al. 2018). In *Lycaeides* butterflies, SVs have been demonstrated to be strongly selected in hybrid zones and contribute to hybrid fitness and reproductive isolation (Zhang et al. 2022). Altogether, these examples and our pan-genome study suggest that TE insertions coupled to gene regulation may be an underappreciated source of variation for natural selection to act upon. We expect that the accumulation of high-quality genome assemblies thanks to long-read sequencing technologies will continue to improve the identification of SVs and highlight their importance in generating adaptive genetic variation.

Materials and methods

Heliconius charithonia haploid genome assemblies

For *Heliconius charithonia*, we extracted high-molecular-weight DNA from a flash frozen pupa obtained from a wild-caught female sampled in San Juan, Puerto Rico using QIAGEN Inc. Genomic-tip 100/G. Library preparation using 10x Chromium technology for linked reads (10x Genomics, San Francisco, USA) and Illumina sequencing was carried out by Novogene Co., Ltd, which generated 44.9 Gb for a target coverage of 100X. We assembled the linked-read sequencing data using the Supernova 2.1.1 assembler (Weisenfeld et al. 2014) using the default recommended settings and a maximum number of reads of 200 million. Raw assembly outputs were transformed to FASTA format using the pseudohap2 option to generate two parallel pseudo-haplotypes from the diploid genome. Quality control of the *H. charithonia* genome was performed using genome-wide statistics calculated on the phase blocks, synteny with the *H. melpomene* v2.5 genome using Tigmint v1.2.3 (Jackman et al. 2018), and using Benchmarking Universal Single-Copy Ortholog (BUSCO) analysis with the lepidoptera_odb10 database to assess genome assembly and annotation completeness (Simão et al. 2015). Fragmented *H. charithonia* scaffolds were ordered with Tigmint using synteny with the *H. melpomene* v2.5 genome.

Pan-genome alignment

In comparison to using a single genome as a reference, a pan-genome represents a composite of different genomes and serves as a global reference with which to make comparisons between genomes (e.g., conservation and unique sequences) or genome features (e.g., gene and TE annotations). We aligned the two newly assembled haploid *H. charithonia* genomes with the *H. e. demophoon* and *H. m. melpomene* genome using seq-seq-pan (Jandrasits et al. 2018). Seq-seq-pan extends the functionality of the multiple genome aligner progressiveMauve (Darling et al. 2010) by constructing a composite consensus or pan-genome that includes both homologous sequences or locally collinear blocks (LCBs) as well as lineage-specific (non-homologous) sequences in each of the genomes. This pan-genome is then used as the reference coordinates space for the multi genome alignment which can then include sequences specific to any of the genomes. We used the *H. e. demophoon* v1 reference genome as the first genome in the genome list so that the resulting pan-genome alignment would be ordered according to the *H. e. demophoon* reference. This resulted in a pan-genome sequence with a total length of 659,350,588 bp. To avoid spurious feature mappings (i.e., TEs and ATAC-seq peaks), we excluded scaffolds that have not been linked to chromosome positions in *H. e. demophoon* in further analyses by cutting the pan-genome alignment at the end of Chromosome 21 (position 578,665,626 in the alignment). The absence and presence of genome sequences in each of the genomes relative to the pan-genome was assessed with a custom Python script that generates a BED file of start and end positions of LCBs and non-homologous sequences. These BED files were used to identify lineage-specific or homologous sequences between genomes using BEDtools v2.27.1 (Quinlan and Hall 2010). Lineage-specific sequences were obtained by first recording sequence coordinates of each genome relative to the pan-genome using a custom Python script and intersecting these coordinates of each genome against a merged library of sequence coordinates of all other genomes using BEDtools.

Transposable Element (TE) annotation and analysis

To identify TEs, we used a two-stage strategy combining the programs RepeatModeler2 (Flynn et al. 2020) and RepeatMasker (Tarailo-Graovac and Chen 2009) using available curated TE libraries as well as novel TE discovery. In the first stage, RepeatModeler 2.0.1 was run on the four genomes for *de novo* identification of TEs, to classify them into families, and merge the results into a single library. We used the Perl script "cleanup_nested.pl" from the LTR_retriever package (Ou and Jiang 2018) with default parameters to reduce redundant and nested TEs. The TE library was then filtered to eliminate all sequences shorter than 200 bp and all sequences that matched any non TE-related genes using a Blast2GO homology search (Conesa et al. 2005) with the insect-only default library (non-redundant protein sequence nr v5). Finally, the filtered TEs were matched with the *Heliconius* specific TE library from Ray *et al.* (2019) using Blast2GO. This library was produced with *de novo* TE annotations of 19 Heliconiinae and including *H. erato* and *H. melpomene*. The remaining sequences with a TE annotation from RepeatModeler that did not match the *Heliconius* specific TE library from Ray *et al.* (2019) were analyzed with different strategies appropriate for the transposon type. First, the putative autonomous elements (DNA, LTR, and LINE) were analyzed with Blast2GO against the insect-only default library. DNA and LTR elements had to have at least a TE-derived transposase and/or match with other DNA/LTR elements. The LINE required the presence of a reverse transcriptase. Second, the putative SINEs were searched in SINEbase (Vassetzky and Kramerov 2013) and accepted only if at least one of their parts (head, body, tail) matched with a SINE element in the database. Third, the putative Helitrons were identified using DeepTE with the parameters -sp M -m M -fam ClassII (Yan et al. 2020). TEs identified as Helitrons were then scanned with CENSOR (Kohany et al. 2006) to confirm their origin. From these analyses we annotated an additional 93 TEs compared to Ray *et al.* (2019). These TEs were labelled as "putative TEs" and were added to the library from Ray *et al.* (2019) to obtain the final library.

In the second stage, we used the non-redundant library as a custom library in RepeatMasker 4.1.0 to annotate the Tes within our genomes. The RepeatMasker results were cleaned with "one code to find them all" (Bailly-Bechet et al. 2014). This script combines fragmented RepeatMasker hits into complete TE copies and solves ambiguous cases of nested TE. We identified TE families that have been differentially active between phylogenetic branches using a chi-square test with false discovery rate correction. We characterized temporal variation of Metulj-7 and Metulj-m51, two TEs that showed the strongest temporal changes in activity, using the percent of divergence compared to the TE library reference sequence obtained from RepeatMasker, corrected with the Jukes-Cantor model. Finally, TE fragmentation was calculated based on the total length of each element recovered from the reference library.

ATAC-seq library preparation

ATAC-seq libraries were constructed as in Lewis and Reed (2019), a protocol modified from Buenrostro et al. (2013), with minor modifications. *H. melpomene rosina* and *H. erato demophoon* butterflies were collected in Gamboa, Panama; *H. charithonia* butterflies were collected in San Juan, Puerto Rico. Two caterpillars of each species were reared on their respective host plants and allowed to grow until the wandering stage at 5th instar. Live larvae were placed on ice for 1-2 minutes and then pinned and dissected in 1X ice cold PBS. Using dissection scissors, the head was removed, and incisions were

461 performed between the mandibles and at the base of the vertexes. Fine forceps were then used to remove
462 the head cuticle to expose the tissue below. The brain and eye-antennal tissue was subsequently dissected
463 out, by removing the remaining cuticle still attached to the tissue. Similarly, developing wings were
464 dissected from the 5th instar caterpillars and the left and right forewing and left and right hindwing were
465 pooled, respectively.

466 The tissues were then submerged in 350 µl of sucrose solution (250mM D-sucrose, 10mM Tris-HCl,
467 1mM. $MgCl_2$, 1x protease inhibitors) inside 2 ml dounce homogenizers for tissue homogenization and
468 nuclear extraction. After homogenizing the tissue on ice, the resulting cloudy solution was centrifuged at
469 1000 rcf for 7 minutes at 4 ˚C. The pellet was then resuspended in 150 µl of cold lysis buffer (10mM
470 Tris-HCl, 10mM NaCl, 3mM $MgCl_2$, 0.1% IGEPAL CA-630 (Sigma-Aldrich), 1x protease inhibitors) to
471 burst the cell membranes and release nuclei into the solution. Samples were then checked under a
472 microscope with a counting chamber following each nuclear extraction, to confirm nuclei dissociation and
473 state and to assess the concentration of nuclei in the sample. Finally based on these observations a
474 calculation to assess the number of nuclei, and therefore DNA, to be exposed to the transposase was
475 performed. This number was fixed on 400,000, as it is the number of nuclei required to obtain the same
476 amount of DNA from a ~0.4 Gb genome, such as that of *H. erato* and *H. charithonia*, as is contained in
477 50,000 human nuclei – the amount of DNA for which ATAC-seq is optimized (Buenrostro et al. 2013).
478 For *H. melpomene* this number was 500,333, where the genome size of *H. melpomene* is 0.275 Gb. For
479 this quality control, a 15 µl aliquot of nuclear suspension was stained with trypan blue, placed on a
480 hemocytometer and imaged at 64x. After confirmation of adequate nuclear quality and assessment of
481 nuclear concentration, a subsample of the volume corresponding to 400,000 nuclei (*H. erato* and *H.*
482 *charithonia*) and 500,333 (*H. melpomene*) was aliquoted, pelleted 1,000 rcf for 7 minutes at 4 ˚C and
483 immediately resuspended in a transposition mix, containing Tn5 enzyme (Illumina DNA Prep) in a
484 transposition buffer. The transposition reaction was incubated at 37 °C for exactly 30 minutes. A PCR
485 Minelute Purification Kit (Qiagen) was used to interrupt the tagmentation and purify the resulting tagged
486 fragments, which were amplified using custom-made Nextera primers and a NEBNext High-fidelity 2x
487 PCR Master Mix (New England Labs). The amplified libraries were quantified on a Qubit, visualized on
488 an Agilent Bioanalyzer 2100 and sequenced as 37 to 76 bp paired-end fragments with NextSeq 500
489 Illumina technology at the Sequencing and Genomics Facility of the University of Puerto Rico
490 (Supplemental Table S6).

491

492 *ATAC-seq data analysis*

493 Raw Illumina reads were filtered for adapters and quality using Trimmomatic v0.39 (Bolger et al. 2014).
494 Filtered reads for each sample were then mapped to their respective reference genome using Bowtie 2
495 v2.2.6 (Langmead and Salzberg 2013) using default parameters. We used SAMtools v1.2 (Li et al. 2009)
496 to sort mapped reads and only retained reads with a mapping Phred score higher than 20 (-q 20) and that
497 were uniquely mapped and properly oriented (-f 0x02). PCR duplicates were identified and removed
498 using Picard-tools v2.5 (http://picard.sourceforge.net).

499 ATAC-seq peak intervals were called on the mapped reads (BAM files) of each sample using the MACS2
500 'callpeak' command with –g set to the respective reference genome size and –shift set to -100 and –
501 extsize set to 200 (Zhang et al. 2008). Peaks were only retained if they occurred in both replicates with a

reciprocal minimal 25% overlap, as determined with BEDtools intersect function. The function 'multicov' from BEDtools was used to obtain read counts within ATAC-seq peaks. These read counts were used to obtain library size scaling factors using the function 'estimateSizeFactors' from the R package DESeq2 (R Core Team 2018; Love et al. 2014) . Next, BAM files were converted to BEDgraphs using the BEDtools function 'genomecov' and scaled using the size scaling factors. Mean ATAC-seq traces for each species were obtained from the two replicate samples using wiggletools (Zerbino et al. 2014). Differential accessibility between head and wing tissues was tested in each species using DESeq2 (Love et al. 2014) with an adjusted p-value smaller than 0.05 and fold change larger than 1.

Feature mapping to pan-genome coordinates and comparisons

Features, including genome sequences that are lineage-specific, TE annotations from RepeatMasker, gene annotations (obtained from *H. e. demophoon*), and ATAC-seq peaks from MACS2 were compared after converting their genome coordinates to pan-genome coordinates. This was done by first using the 'map' utility of the seq-seq-pan software (Jandrasits et al. 2018) and custom scripts. Features that overlapped with scaffold starts or ends in any of the genomes were masked using BEDtools 'subtract' (-A) to avoid including results from fragmented or missing sequences. Next, lineage-specific sequences were intersected with TE annotations and ATAC-seq peaks using BEDtools 'intersect'. We only considered ATAC-seq peaks (with an average size of 500.45 bp (*sd* = 283.57)) that were completely within an SV to be considered resulting from SV. ATAC-seq analyses are thus performed on the faction of SVs larger than 50 bp. Lineage-specific sequences in one of the genomes that did not match a TE annotation were identified as duplications when identifying a BLAST hit with a similarity higher than 70% elsewhere in the genome using BLAST v2.10.0.

Feature distribution

We measured the genomic distance along the pan-genome of lineage-specific sequences, TEs and ATAC-seq peaks from the closest transcription start site (TSS) of a gene using the function 'annotatePeaks' from the software suite HOMER (Heinz et al. 2010). Each distribution was compared with that of 100,000 random positions with a pairwise Wilcoxon test. For each distribution pair an overlapping index was measured, using the R package *overlapping* v1.6 (Pastore 2018).

Motif enrichment

Differential motif enrichment analysis was performed for ATAC-seq peaks that overlapped with lineage-specific TEs using the STREME tool from the MEME suite (Machanick and Bailey 2011; Bailey 2021). This was done for four phylogenetic comparisons: *H. charithonia* compared to *H. erato, H. charithonia* compared to *H. melpomene, H. erato* compared to *H. melpomene,* and *H. melpomene* compared to *H. erato.* As a background model, we constructed a custom dataset including a combined set of lineage-specific TEs without ATAC-seq peaks from the phylogenetic comparisons. Motifs with a p-value smaller than 0.001 were analyzed with Tomtom from the MEME-suite to identify motifs similar transcription factor binding sites in *Drosophila melanogaster* (Gupta et al. 2007).

Historical population demography

Changes in historical population sizes from individual genome sequences were inferred using the pairwise sequentially Markovian coalescent (PSMC) as implemented in MSMC (Schiffels and Durbin 2014). Genotypes were inferred using SAMtools v0.1.19 (Li et al. 2009) from reads mapped to the respective reference genomes using BWA v0.7 (Li and Durbin 2010). This involved a minimum mapping (-q) and base (-Q) quality of 20 and adjustment of mapping quality (-C) 50. A mask file was generated for regions of the genome with a minimum coverage depth of 30 and was provided together with heterozygosity calls to the MSMC tool. MSMC was run on heterozygosity calls from all contiguous scaffolds longer than 500 kb, excluding scaffolds on the Z Chromosome. We scaled the PSMC estimates using a generation time of 0.25 years and a mutation rate of 2e-9 as estimated for *H. melpomene* (i.e., spontaneous *Heliconius* mutation rate corrected for selective constraint (Keightley et al. 2014; Martin et al. 2015)). We obtained whole-genome resequencing reads for *H. e. demophoon* and *H. m. melpomene* from two individuals each from Panama (SAMN05224182, SAMN05224183, SAMEA1919255, and SAMEA1919258 from Van Belleghem et al. 2018). For *H. charithonia*, we obtained resequencing data for one sample from Panama (SAMN05224120 from Van Belleghem et al. 2017) and two samples from Puerto Rico (SAMN05224121 from Van Belleghem *et al.* (2017) and one using the 10x linked-read sequencing data used for the genome assembly from the Puerto Rican population).

Signatures of selective sweeps

SweepFinder2 (Degiorgio et al. 2016) was used to detect signatures of selective sweeps in genomic regions with ATAC-seq peaks with lineage-specific TEs. Genotypes from 10 *H. erato demophoon* and 10 *H. melpomene rosina* individuals from Panamanian populations were obtained from Van Belleghem et al. (2018). Allele counts for biallelic SNPs were generated using a custom Python script. SNPs were polarized using *H. hermathena* and *H. numata* for the *H. erato* and *H. melpomene* population, respectively. SweepFinder2 was run using default settings and set to test SNPs every 2000 bp (-sg 2000).

Data access

The 10x chromium sequencing and ATAC-seq raw read data generated in this study have been submitted to the NCBI BioProject database (https://www.ncbi.nlm.nih.gov/bioproject/) under accession number PRJNA795145 (SAMN24661992 and SAMN24689923-SAMN24689940). The *H. charithonia* pseudo-haplotypes have been deposited at DDBJ/ENA/GenBank under accession number JAKFBP000000000. Code for analyses is available as Supplemental Material and at https://github.com/StevenVB12/Genomics.

Competing interest statement

The authors declare no competing interests.

Acknowledgements

We thank Christine Jandrasits for advice in using seq-seq-pan, Markus Möst for help with running SweepFinder2 and Simon H. Martin for help in interpreting chromosomal indel diversity patterns. We also thank Silvia Planas from the Sequencing and Genomics Facility of the University of Puerto Rico-Rio Piedras for their assistance with genome and ATAC-seq library preparation and sequencing. This work was supported by a National Institutes of Health-4 NIGMS COBRE Phase 2 Award – Center for Neuroplasticity at the University of Puerto Rico (Grant No. 1P20GM103642) to SMVB, a Puerto Rico Science, Technology & Research Trust catalyzer award (#2020-00142) to SMVB and RP, and an NSF EPSCoR RII Track-2 FEC (grant no. OIA 1736026), an NSF IOS 1656389, and a Fondo Institucional para la Investigacio´n (FIPI), Universidad de Puerto Rico - Recinto de Río Piedras, Decanato de Estudios Graduados e Investigación to RP. For sequencing and computational resources, we thank the University of Puerto Rico Sequencing and Genomics Facility INBRE Grant P20 GM103475 from the National Institute for General Medical Sciences (NIGMS), a component of the National Institutes of Health (NIH), and the Bioinformatics Research Core of the INBRE. Its contents are solely the responsibility of the authors and do not necessarily represent the official view of NIGMS or NIH.

Author Contributions: This study was conceived and designed by SMVB with contributions from AAR, RP, JJL, LL, BAC, WOM, CDJ, JARM, AG and SHM. SMVB and AAR analyzed the data. LL, LH, YOR, EE and SMVB collected ATAC-seq data. YOR and SMVB performed genome sequencing. FC performed genome quality analyses. AAR and SMVB wrote the initial manuscript with input and edits from all authors.

References

Ashraf S, Hu X, Roote J, Ip Y. 1999. The mesoderm determinant Snail collaborates with related zinc-finger proteins tocontrol Drosophila neurogenesis. *EMBO J* **18**: 6426–6438.

Ashraf SI, Ganguly A, Roote J, Ip YT. 2004. Worniu, a snail family zinc-finger protein, is required for brain development in *Drosophila*. *Dev Dyn* **231**: 379–386.

Bailey TL. 2021. STREME: accurate and versatile sequence motif discovery. *Bioinformatics* **37**: 2834–2840.

Bailly-Bechet M, Haudry A, Lerat E. 2014. "One code to find them all": A perl tool to conveniently parse RepeatMasker output files. *Mob DNA* **5**: 1–15.

Baxter SW, Nadeau NJ, Maroja LS, Wilkinson P, Counterman B a, Dawson A, Beltran M, Perez-Espona S, Chamberlain N, Ferguson L, et al. 2010. Genomic hotspots for adaptation: the population genetics of Müllerian mimicry in the Heliconius melpomene clade. *PLoS Genet* **6**: e1000794.

Beltrán M, Jiggins C, Brower A, Bermingham E, Mallet J. 2007. Do pollen feeding and pupal-mating have a single origin in *Heliconius* butterflies? Inferences from multilocus sequence data. *Biol J Linn Soc* **92**: 221–239.

Bolger AM, Lohse M, Usadel B. 2014. Trimmomatic: A flexible trimmer for Illumina sequence data. *Bioinformatics* **30**: 2114–2120.

Bourque G, Burns KH, Gehring M, Gorbunova V, Seluanov A, Hammell M, Imbeault M, Izsvák Z, Levin HL, Macfarlan TS, et al. 2018. Ten things you should know about transposable elements. *Genome Biol* **19**: 1–12.

Branco MR, Chuong EB. 2020. Crossroads between transposons and gene regulation. *Philos Trans R Soc B Biol Sci* **375**: 2–5.

Brown K. 1981. The biology of *Helcionius* and related genera. *Annu Rev Entomol* **26**: 427–456.

Buenrostro J, Giresi P, Zaba L, Chang H, Greenleaf W. 2013. Transposition of native chromatin for multimodal regulatory analysis and personal epigenomics. *Nat Methods* **10**: 1213–1218.

Calcino AD, Kenny NJ, Gerdol M. 2021. Single individual structural variant detection uncovers widespread hemizygosity in molluscs. *Philos Trans R Soc B Biol Sci* **376**: 20200153.

Campos JL, Charlesworth B. 2019. The effects on neutral variability of recurrent selective sweeps and background selection. *Genetics* **212**: 287–303.

Cerbin S, Jiang N. 2018. Duplication of host genes by transposable elements. *Curr Opin Genet Dev* **49**: 63–69.

Charlesworth B. 2009. Effective population size and patterns of molecular evolution and variation. *Nat Rev Genet* **10**: 195–205.

Charlesworth B. 2001. The effect of life-history and mode of inheritance on neutral genetic variability. *Genet Res* **77**: 153–166.

Cicconardi F, Lewis JJ, Martin SH, Reed RD, Danko CG, Montgomery SH. 2021. Chromosome Fusion Affects Genetic Diversity and Evolutionary Turnover of Functional Loci but Consistently Depends on Chromosome Size. *Mol Biol Evol* **38**: 4449–4462.

Cicconardi F, Milanetti E, Pinheiro de Castro E, Mazo-vargas A, SM VB, Ruggieri A, Rastas P, Hanly J, Evans E, Jiggins C, et al. 2022. Evolutionary dynamics of genome size and content during the adaptive radiation of Heliconiini butterflies. *bioRxiv*.

Collins RL, Brand H, Karczewski KJ, Zhao X, Alföldi J, Francioli LC, Khera A V., Lowther C, Gauthier LD, Wang H, et al. 2020. A structural variation reference for medical and population genetics. *Nature* **581**: 444–451.

Conesa A, Götz S, García-Gómez JM, Terol J, Talón M, Robles M. 2005. Blast2GO: A universal tool for annotation, visualization and analysis in functional genomics research. *Bioinformatics* **21**: 3674–3676.

Cutter AD, Payseur BA. 2013. Genomic signatures of selection at linked sites: Unifying the disparity among species. *Nat Rev Genet* **14**: 262–274.

Darling AE, Mau B, Perna NT. 2010. Progressivemauve: Multiple genome alignment with gene gain, loss and rearrangement. *PLoS One* **5**: e11147.

Davey JW, Barker SL, Rastas PM, Pinharanda A, Martin SH, Durbin R, McMillan WO, Merrill RM, Jiggins CD. 2017. No evidence for maintenance of a sympatric *Heliconius* species barrier by chromosomal inversions. *Evol Lett* **1**: 138–154.

Davey JW, Chouteau M, Barker SL, Maroja L, Baxter SW, Simpson F, Merrill RM, Joron M, Mallet J, Dasmahapatra KK, et al. 2016. Major improvements to the *Heliconius melpomene* genome assembly used to confirm 10 chromosome fusion events in 6 million years of butterfly evolution. *G3 Genes|Genomes|Genetics* **6**: 695–708.

Davies N, Bermingham E. 2002. The historical biogeography of two Caribbean butterflies (Lepidoptera: Heliconiidae) as inferred from genetic variation at multiple loci. *Evolution (N Y)* **56**: 573–589.

Degiorgio M, Huber CD, Hubisz MJ, Hellmann I, Nielsen R. 2016. SweepFinder2: Increased sensitivity, robustness and flexibility. *Bioinformatics* **32**: 1895–1897.

Diehl AG, Ouyang N, Boyle AP. 2020. Transposable elements contribute to cell and species-specific chromatin looping and gene regulation in mammalian genomes. *Nat Commun* **11**: 1–18.

Ebert P, Audano PA, Zhu Q, Rodriguez-Martin B, Porubsky D, Bonder MJ, Sulovari A, Ebler J, Zhou W, Mari RS, et al. 2021. Haplotype-resolved diverse human genomes and integrated analysis of structural variation. *Science (80-)* **372**.

Ecco G, Imbeault M, Trono D. 2017. KRAB zinc finger proteins. *Development* **144**: 2719–2729.

Edelman NB, Frandsen PB, Miyagi M, Clavijo B, Davey J, Dikow R, García-accinelli G, Van Belleghem SM, Patterson N, Daniel E, et al. 2019. Genomic architecture and introgression shape a butterfly radiation. *Science (80-)* **366**: 24174–24183.

Flynn JM, Hubley R, Goubert C, Rosen J, Clark AG, Feschotte C, Smit AF. 2020. RepeatModeler2 for automated genomic discovery of transposable element families. *Proc Natl Acad Sci U S A* **117**: 9451–9457.

Fueyo R, Judd J, Feschotte C, Wysocka J. 2022. Roles of transposable elements in the regulation of mammalian transcription. *Nat Rev Mol Cell Biol* **24**: 19–24.

Garcia-Perez JL, Widmann TJ, Adams IR. 2016. The impact of transposable elements on mammalian development. *Dev* **143**: 4101–4114.

Gerdol M, Moreira R, Cruz F, Gómez-Garrido J, Vlasova A, Rosani U, Venier P, Naranjo-Ortiz MA, Murgarella M, Greco S, et al. 2020. Massive gene presence-absence variation shapes an open pan-genome in the Mediterranean mussel. *Genome Biol* **21**: 275.

Guo X, Yin C, Yang F, Zhang Y, Huang H, Wang J, Deng B, Cai T, Rao Y, Xi R. 2019. The cellular diversity and transcription factor code of *Drosophila* enteroendocrine cells. *Cell Rep* **29**: 4172-4185.e5.

Gupta S, Stamatoyannopoulos JA, Bailey TL, Noble WS. 2007. Quantifying similarity between motifs. *Genome Biol* **8**.

Heinz S, Benner C, Spann N, Bertolino E, Lin YC, Laslo P, Cheng JX, Murre C, Singh H, Glass CK. 2010. Simple combinations of lineage-determining transcription factors prime cis-regulatory elements required for macrophage and B cell identities. *Mol Cell* **38**: 576–589.

Hendrickx F, Corte Z De, Sonet G, Belleghem SM Van, Köstlbacher S, Vangestel C. 2022. A masculinizing supergene underlies an exaggerated male reproductive morph in a spider. *Nat Ecol Evol* **6**: 195–206.

Hill WG, Robertson A. 1966. The effect of linkage on limits to artificial selection. *Genet Res (Camb)* **8**: 269–294.

Hübner S, Bercovich N, Todesco M, Mandel JR, Odenheimer J, Ziegler E, Lee JS, Baute GJ, Owens GL, Grassa CJ, et al. 2019. Sunflower pan-genome analysis shows that hybridization altered gene content and disease resistance. *Nat Plants* **5**: 54–62.

Iijima T, Kajitani R, Komata S, Lin CP, Sota T, Itoh T, Fujiwara H. 2018. Parallel evolution of Batesian mimicry supergene in two *Papilio* butterflies, *P. polytes* and *P. memnon*. *Sci Adv* **4**: eaao5416.

Iyer EPR, Iyer SC, Sullivan L, Wang D, Meduri R, Graybeal LL, Cox DN. 2013. Functional genomic Analyses of two morphologically distinct classes of *Drosophila* sensory neurons: Post-mitotic roles of transcription factors in dendritic patterning. *PLoS One* **8**.

Jackman SD, Coombe L, Chu J, Warren RL, Vandervalk BP, Yeo S, Xue Z, Mohamadi H, Bohlmann J, Jones SJM, et al. 2018. Tigmint: Correcting assembly errors using linked reads from large molecules. *BMC Bioinformatics* **19**: 1–10.

Jandrasits C, Dabrowski PW, Fuchs S, Renard BY. 2018. Seq-seq-pan: Building a computational pan-genome data structure on whole genome alignment. *BMC Genomics* **19**: 1–12.

Jay P, Chouteau M, Whibley A, Bastide H, Parrinello H, Llaurens V, Joron M. 2021. Mutation load at a mimicry supergene sheds new light on the evolution of inversion polymorphisms. *Nat Genet* **53**: 288–293.

Jiggins CD. 2017. *The ecology and evolution of* Heliconius *butterflies*. Oxford University Press.

Joly-Lopez Z, Bureau TE. 2018. Exaptation of transposable element coding sequences. *Curr Opin Genet Dev* **49**: 34–42.

Joron M, Frezal L, Jones RT, Chamberlain NL, Lee SF, Haag CR, Whibley A, Becuwe M, Baxter SW, Ferguson L, et al. 2011. Chromosomal rearrangements maintain a polymorphic supergene controlling butterfly mimicry. *Nature* **477**: 203–206.

Keightley PD, Pinharanda A, Ness RW, Simpson F, Dasmahapatra KK, Mallet J, Davey JW, Jiggins CD. 2014. Estimation of the spontaneous mutation rate in *Heliconius melpomene*. *Mol Biol Evol* **32**: 239–243.

Kohany O, Gentles AJ, Hankus L, Jurka J. 2006. Annotation, submission and screening of repetitive elements in Repbase: RepbaseSubmitter and Censor. *BMC Bioinformatics* **7**: 1–7.

Kozak KM, Wahlberg N, Neild AFE, Dasmahapatra KK, Mallet J, Jiggins CD. 2015. Multilocus species trees show the recent adaptive radiation of the mimetic *Heliconius* butterflies. *Syst Biol* **64**: 505–524.

Kozlov A, Jaumouillé E, Almeida PM, Koch R, Rodriguez J, Abruzzi KC, Nagoshi E. 2017. A screening of UNF targets identifies Rnb, a novel regulator of Drosophila circadian rhythms. *J Neurosci* **37**: 6673–6685.

Langmead B, Salzberg SL. 2013. Fast gapped-read alignment with Bowtie 2. *Nat Methods* **9**: 357–359.

Lavoie CA, Ii RNP, Novick PA, Counterman BA, Ray DA. 2013. Transposable element evolution in *Heliconius* suggests genome diversity within Lepidoptera. *Mob DNA* **4**: 1–10.

Leffler EM, Bullaughey K, Matute DR, Meyer WK, Ségurel L, Venkat A, Andolfatto P, Przeworski M. 2012. Revisiting an old riddle: What determines genetic diversity levels within species? *PLoS Biol* **10**: e1001388.

Lewis JJ, Geltman RC, Pollak PC, Rondem KE, Belleghem SM Van. 2019. Parallel evolution of ancient, pleiotropic enhancers underlies butterfly wing pattern mimicry. *Proc Natl Acad Sci* **116**: 24174–24183.

Lewis JJ, Reed RD. 2019. Genome-wide regulatory adaptation shapes population-level genomic landscapes in *Heliconius* ed. P. Wittkopp. *Mol Biol Evol* **36**: 159–173.

Lewis JJ, Van Belleghem SM, Papa R, Danko CG, Reed RD. 2020. Many functionally connected loci foster adaptive diversification along a neotropical hybrid zone. *Sci Adv* **6**: 1–11.

Li H, Durbin R. 2010. Fast and accurate long-read alignment with Burrows-Wheeler transform. *Bioinformatics* **26**: 589–595.

Li H, Handsaker B, Wysoker A, Fennell T, Ruan J, Homer N, Marth G, Abecasis G, Durbin R. 2009. The Sequence Alignment/Map format and SAMtools. *Bioinformatics* **25**: 2078–2079.

Liu Y, Ramos-Womack M, Han C, Reilly P, Brackett KLR, Rogers W, Williams TM, Andolfatto P, Stern DL, Rebeiz M. 2019. Changes throughout a genetic network Mask the contribution of Hox gene evolution. *Curr Biol* **29**: 2157-2166.e6.

Livraghi L, Hanly J, Van Belleghem S, Montejo-Kovacevich G, van der Heijden E, Loh LS, Ren A, Warren I, Lewis J, Concha C, et al. 2021. *Cortex cis*-regulatory switches establish scale colour identity and pattern diversity in *Heliconius*. *Elife* **10**: e68549.

Love MI, Huber W, Anders S. 2014. Moderated estimation of fold change and dispersion for RNA-seq data with DESeq2. *Genome Biol* **15**: 1–21.

Lucek K, Gompert Z, Nosil P. 2019. The role of structural genomic variants in population differentiation and ecotype formation in Timema cristinae walking sticks. *Mol Ecol* **28**: 1224–1237.

Machanick P, Bailey TL. 2011. MEME-ChIP: Motif analysis of large DNA datasets. *Bioinformatics* **27**: 1696–1697.

Mallarino R, Henegar C, Mirasierra M, Manceau M, Schradin C, Vallejo M, Beronja S, Barsh GS, Hoekstra HE. 2016. Developmental mechanisms of stripe patterns in rodents. *Nature* **539**: 518–523.

Mallet J, Gilbert L. 1995. Why are there so many mimicry rings? Correlations between habitat, behaviour and mimicry in *Heliconius* butterflies. *Biol J Linn Soc* **55**: 159–180.

Martin SH, Davey JW, Salazar C, Jiggins CD. 2019. Recombination rate variation shapes barriers to introgression across butterfly genomes. *PLOS Biol* **17**: e2006288.

Martin SH, Eriksson A, Kozak KM, Manica A, Jiggins CD. 2015. Speciation in Heliconius Butterflies□: Minimal Contact Followed by Millions of Generations of Hybridisation. *BioRxiv* 1–24.

Matschiner M, Barth JMI, Tørresen OK, Star B, Baalsrud HT, Brieuc MSO, Pampoulie C, Bradbury I, Jakobsen KS, Jentoft S. 2022. Supergene origin and maintenance in Atlantic cod. *Nat Ecol Evol*.

Mendoza-Cuenca L, MacÍas-Ordóñez R. 2010. Female asynchrony may drive disruptive sexual selection on male mating phenotypes in a Heliconius butterfly. *Behav Ecol* **21**: 144–152.

Mérot C, Oomen RA, Tigano A, Wellenreuther M. 2020. A roadmap for understanding the evolutionary significance of structural genomic variation. *Trends Ecol Evol* **35**: 561–572.

Moest M, Van Belleghem SM, James J, Salazar C, Martin S, Barker S, Moreira G, Mérot C, Joron M, Nadeau N, et al. 2020. Selective sweeps on novel and introgressed variation shape mimicry loci in a butterfly adaptive radiation. *PLoS Biol* **18**: e3000597.

Montgomery S, Rossi M, WO M, Merrill R. 2021. Neural divergence and hybrid disruption between ecologically isolated *Heliconius* butterflies. *Proc Natl Acad Sci* **118**: e2015102118.

Montgomery SH, Merrill RM. 2017. Divergence in brain composition during the early stages of ecological specialization in Heliconius butterflies. *J Evol Biol* **30**: 571–582.

Nishikawa H, Iijima T, Kajitani R, Yamaguchi J, Ando T, Suzuki Y, Sugano S, Fujiyama A, Kosugi S, Hirakawa H, et al. 2015. A genetic mechanism for female-limited Batesian mimicry in Papilio butterfly. *Nat Genet* **47**: 405–409.

Ohtani H, Iwasaki Y. 2021. Rewiring of chromatin state and gene expression by transposable elements. *Dev Growth Differ*.

Okamoto H, Hirochika H. 2001. Silencing of transposable elements in plants. *Trends Plant Sci* **6**: 527–534.

Ou S, Jiang N. 2018. *LTR_retriever: A highly accurate and sensitive program for identification of long terminal repeat retrotransposons*.

Pastore M. 2018. Overlapping: a R package for Estimating Overlapping in Empirical Distributions. *J Open Source Softw* **3**: 1023.

Pinharanda A, Martin SH, Barker SL, Davey JW, Jiggins CD. 2017. The comparative landscape of duplications in *Heliconius melpomene* and *Heliconius cydno*. *Heredity (Edinb)* **118**: 78–87.

Plissonneau C, Hartmann FE, Croll D. 2018. Pangenome analyses of the wheat pathogen *Zymoseptoria tritici* reveal the structural basis of a highly plastic eukaryotic genome. *BMC Biol* **16**: 1–16.

Poelstra JW, Vijay N, Hoeppner MP, Wolf JBW. 2015. Transcriptomics of colour patterning and coloration shifts in crows. *Mol Ecol* **24**: 4617–4628.

Pontis J, Planet E, Offner S, Turelli P, Duc J, Coudray A, Theunissen TW, Jaenisch R, Trono D. 2019. Hominoid-specific transposable elements and KZFPs facilitate human embryonic genome activation and control transcription in naive human ESCs. *Cell Stem Cell* **24**: 724-735.e5.

Quinlan AR, Hall IM. 2010. BEDTools: a flexible suite of utilities for comparing genomic features. *Bioinformatics* **26**: 841–2.

R Core Team. 2018. R: A language and environment for statistical computing. https://www.r-project.org/.

Ray DA, Grimshaw JR, Halsey MK, Korstian JM, Osmanski AB, Sullivan KAM, Wolf KA, Reddy H, Foley N, Stevens RD, et al. 2019. Simultaneous TE Analysis of 19 Heliconiine Butterflies Yields Novel Insights into Rapid TE-Based Genome Diversification and Multiple SINE Births and Deaths. *Genome Biol Evol* **11**: 2162–2177.

Read BA, Kegel J, Klute MJ, Kuo A, Lefebvre SC, Maumus F, Mayer C, Miller J, Monier A, Salamov A, et al. 2013. Pan genome of the phytoplankton *Emiliania* underpins its global distribution. *Nature* **499**: 209–213.

Reed RD, Chen PH, Frederik Nijhout H. 2007. Cryptic variation in butterfly eyespot development: The importance of sample size in gene expression studies. *Evol Dev* **9**: 2–9.

Rigal M, Mathieu O. 2011. A “mille-feuille” of silencing: Epigenetic control of transposable elements. *Biochim Biophys Acta - Gene Regul Mech* **1809**: 452–458.

Rodriguez-Caro F, Fenner J, Bhardwaj S, Cole J, Benson C, Colombara AM, Papa R, Brown MW, Martin A, Range RC, et al. 2021. Novel *doublesex* duplication associated with sexually dimorphic development of Dogface butterfly wings. *Mol Biol Evol* **38**: 5021–5033.

Sato A, Tomlinson A. 2007. Dorsal-ventral midline signaling in the developing *Drosophila* eye. *Development* **134**: 659–667.

Schiffels S, Durbin R. 2014. Inferring human population size and separation history from multiple genome sequences. *Nat Genet* **46**: 919–925.

Schrader L, Schmitz J. 2019. The impact of transposable elements in adaptive evolution. *Mol Ecol* **28**: 1537–1549.

Simão FA, Waterhouse RM, Ioannidis P, Kriventseva E V. 2015. BUSCO: assessing genome assembly and annotation completeness with single-copy orthologs. *Bioinformatics* **31**: 3210–3212.

Suntsova M V., Buzdin AA. 2020. Differences between human and chimpanzee genomes and their implications in gene expression, protein functions and biochemical properties of the two species. *BMC Genomics* **21**: 1–12.

Tarailo-Graovac M, Chen N. 2009. Using RepeatMasker to identify repetitive elements in genomic sequences. *Curr Protoc Bioinforma* **Chapter 4**: Unit 4.10.

The Chimpanzee Sequencing and Analysis Consortium. 2005. Initial sequence of the chimpanzee genome and comparison with the human genome. *Nature* **437**: 69–87.

Thurman TJ, Brodie E, Evans E, McMillan WO. 2018. Facultative pupal mating in Heliconius erato: Implications for mate choice, female preference, and speciation. *Ecol Evol* 1–8.

Van't Hof AE. 2016. The industrial melanism mutation in British peppered moths is a transposable element. *Nature* **534**: 102–105.

Van Belleghem SM, Baquero M, Papa R, Salazar C, Mcmillan WO, Counterman BA, Jiggins CD, Martin SH. 2018. Patterns of Z chromosome divergence among Heliconius species highlight the importance of historical demography. *Mol Ecol* **27**: 3852–3872.

Van Belleghem SM, Rastas P, Papanicolaou A, Martin SH, Arias CF, Supple MA, Hanly JJ, Mallet J, Lewis JJ, Hines HM, et al. 2017. Complex modular architecture around a simple toolkit of wing pattern genes. *Nat Ecol Evol* **1**: 52.

Vassetzky NS, Kramerov DA. 2013. SINEBase: A database and tool for SINE analysis. *Nucleic Acids Res* **41**: 83–89.

Villar D, Berthelot C, Aldridge S, Rayner TF, Lukk M, Pignatelli M, Park TJ, Deaville R, Erichsen JT, Jasinska AJ, et al. 2015. Enhancer evolution across 20 mammalian species. *Cell* **160**: 554–566.

Weisenfeld NI, Yin S, Sharpe T, Lau B, Hegarty R, Holmes L, Sogoloff B, Tabbaa D, Williams L, Russ C, et al. 2014. Comprehensive variation discovery in single human genomes. *Nat Genet* **46**: 1350–1355.

Weissensteiner MH, Bunikis I, Catalán A, Francoijs KJ, Knief U, Heim W, Peona V, Pophaly SD, Sedlazeck FJ, Suh A, et al. 2020. Discovery and population genomics of structural variation in a songbird genus. *Nat Commun* **11**: 1–11.

Wellenreuther M, Mérot C, Berdan E, Bernatchez L. 2019. Going beyond SNPs: The role of structural genomic variants in adaptive evolution and species diversification. *Mol Ecol* **28**: 1203–1209.

Westerman EL, Vankuren NW, Massardo D, Buerkle N, Palmer SE, Kronforst MR. 2018. *Aristaless* controls butterfly wing color variation used in mimicry and mate choice. *Curr Biol* **28**: 1–6.

Wimmer E, Jäckle H, C P, SM C. 2010. A *Drosophila* homologue of human Sp1 is a head-specific segmentation gene. *J Am Chem Soc* **132**: 2517–2528.

Woronik A, Tunström K, Perry MW, Neethiraj R, Stefanescu C, Celorio-Mancera M de la P, Brattström O, Hill J, Lehmann P, Käkelä R, et al. 2019. A transposable element insertion is associated with an alternative life history strategy. *Nat Commun* **10**. g/10.1038/s41467-019-13596-2.

Yan H, Bombarely A, Li S. 2020. DeepTE: A computational method for de novo classification of transposons with convolutional neural network. *Bioinformatics* **36**: 4269–4275.

Zerbino DR, Johnson N, Juettemann T, Wilder SP, Flicek P. 2014. WiggleTools: Parallel processing of large collections of genome-wide datasets for visualization and statistical analysis. *Bioinformatics* **30**: 1008–1009.

Zhang L, Chaturvedi S, Nice CC, Lucas LK, Gompert Z. 2022. Population genomic evidence of selection on structural variants in a natural hybrid zone. *Mol Ecol*.

Zhang L, Reifová R, Halenková Z, Gompert Z. 2021. How important are structural variants for speciation? *Genes (Basel)* **12**.

Zhang Y, Liu T, Meyer CA, Eeckhoute J, Johnson DS, Bernstein BE, Nussbaum C, Myers RM, Brown M, Li W, et al. 2008. Model-based analysis of ChIP-Seq (MACS). *Genome Biol* **9**.

Figure legends

Figure 1. Genome divergence, lineage-specific sequence distribution and historical demography of *H. melpomene*, *H. erato* and *H. charithonia* from Panama and Puerto Rico. (A.) Phylogenetic relations, genome sizes and approximate divergence times. Colored lines indicate branches investigated in panel D. **(B.)** Inference of historical effective population size changes using pairwise sequentially Markovian coalescent (PSMC) analysis. The PSMC estimates are scaled using a generation time of 0.25 years and a mutation rate of 2e-9. Note that the *H. charithonia* genome was obtained from the Puerto Rican population. **(C.)** Venn diagrams represent homologous and non-homologous (lineage-specific) genomic sequences (excluding Ns). Between the two pseudo-haplotypes of the *H. charithonia* genome, we observed a total of 72.7 Mb of sequence identified as indel. Of these indels, 63.1 Mb (86.8%) were lineage-specific to *H. charithonia*, whereas 9.6 Mb (13.2%) were present in the *H. erato* genome. Consistent with divergence times, the *H. charithonia* genome comprised 43.5% (175.2 Mb; compared to the ~6 MY divergent *H. erato*) to 62.7% (252.3 Mb; compared to the ~11 MY divergent *H. melpomene*) of lineage-specific sequence resulting from SVs. *Heliconius erato* had 39.0% (151.2 Mb) lineage-specific sequences compared to *H. charithonia* and 58.0% (222.1 Mb) lineage-specific sequences compared to *H. melpomene*. *Heliconius melpomene* had 34.5% (95.0 Mb) lineage-specific genomic sequence compared to *H. erato* and *H. charithonia*. **(D.)** Length distribution of lineage-specific sequences. Colored histograms show the frequency of SVs for different phylogenetic comparisons (as indicated in panel A). The black line shows the frequency distribution of lineage-specific SVs that were characterized as transposable elements (TEs). Between the two *H. charithonia* haplotypes, indels had an average and median length of 13.5 and 2 bp. The average and median length was 34.2 and 4 bp for lineage-specific *H. charithonia* sequences relative to *H. erato* and 45.6 and 6 bp relative to *H. melpomene*.

Figure 2. Phylogenetic dynamic of Transposable Elements (TEs). (A) Lineage-specific TE family accumulation. Different line types depict different branches in the phylogeny studied and allow to investigate changes in temporal accumulation of TEs. 1 = TE families associated with indels between the *H. charithonia* haplotypes, 2 = TE families accumulated in *H. charithonia* since the split from *H. erato*, 3 = TE families accumulated in *H. erato* since the split from *H. charithonia*, 4 = TE families accumulated in the *H. erato* lineage since their split from a common ancestor with *H. melpomene*, 5 = TE families accumulated after the *H. charithonia/H. erato* lineage split from the common ancestor with *H. melpomene* but before *H. erato* and *H. charithonia* split, 6= TE families accumulated in the *H. charithonia/H. erato* lineage since their split from a common ancestor with *H. melpomene*. *DNA* = DNA transposons that do not involve an RNA intermediate; *LINE* = long interspersed nuclear elements, which encode reverse transcriptase but lack LTRs; *LTR* = long terminal repeats, which encode reverse transcriptase; *RC* = transpose by rolling-circle replication via a single-stranded DNA intermediate (Helitrons); *SINE* = short interspersed nuclear elements that do not encode reverse transcriptase. **(B.)** Difference in TEs (percentage of total) between branches in the phylogeny considering the same 48 most significantly divergent TE families. Positive values indicate higher accumulation in the first branch, negative values indicated higher accumulation in the second branch of the comparison. Total TE accumulation patterns per lineage are shown in Supplemental Fig. S1. **(C.)** Difference in TEs (percentage of total) between the two *H. charithonia* haplotypes considering the same 48 most significantly divergent TE families.

Figure 3. Patterns of lineage-specific sequence distribution and chromosome lengths. (A.) Correlation between chromosome lengths and SNP frequency (nucleotide diversity, π) for *H. charithonia* and *H. erato*. *Heliconius charithonia* SNPs were obtained by comparing the two genome pseudo-haplotypes. The *H. erato* SNPs were obtained from whole genome resequence data of ten *H. e. demophoon* samples from Panama. Note that the higher nucleotide diversity in *H. erato* likely results from its larger populations size. **(B.)** Correlation between chromosome lengths when only considering homologous sequence and substitutions (pairwise nucleotide differences, D_{xy}) averaged for each chromosome between *H. charithonia* and *H. erato* and *H. melpomene*, respectively. $D_{xy}$was calculated from homologous sequences in the pan-genome. **(C.)** Correlation between homologous chromosome lengths and frequency of indels in the chromosomes of *H. charithonia*. Correlation between homologous chromosome lengths and frequency of lineage-specific sequences in the chromosomes of **(D.)** *H. charithonia* compared to *H. erato*, **(E.)** *H. charithonia* compared to *H. melpomene*, and **(F.)** *H. melpomene* compared to *H. charithonia*. Dashed lines indicate regression fit. Numbers indicate chromosome numbers. Colors refer to sequences specific to *H. charithonia* (pink), *H. erato* (blue) and *H. melpomene* (orange). See Supplemental Fig. S2 for pattern in 1 bp indels, SVs between 2 and 50 bp, SVs larger than 1,000 bp and SVs characterized as TEs.

Figure 4. Lineage-specific sequences and their relationship with chromatin accessibility and gene distribution. **(A.)** Correlation of gene density in 100-kb windows with frequency of transposable elements (TEs). **(B.)** Density plot of distance of lineage-specific TEs to closest transcription start site (TSS) pooled over all species genome comparisons. **(C.)** Lineage-specific and shared open chromatin signals (ATAC-seq peaks) found in head tissue of 5th instar caterpillars in each species. Peaks are considered shared (homologous) when they overlap at least 50% reciprocally. **(D.)** Correlation of gene frequency in 100-kb windows with frequency of all lineage-specific structural variants (SVs), all ATAC-seq peaks, lineage-specific ATAC-seq peaks, and lineage-specific TE insertions with ATAC-seq peaks. **(E.)** Density plot of distance of lineage-specific sequence features to closest transcription start site (TSS) pooled over all species genome comparisons. We found the distribution of lineage-specific SVs was most similar to a random distribution of positions in the genome (overlapping index = 95%), with a median/mean distance of 21,701/40,790 bp of a lineage-specific sequence and 20,801/39,908 bp of any random position to a TSS. **(F.)** Density plot of distance of lineage-specific TEs with ATAC-seq peaks in *H. charithonia* to closest TSS. Dashed lines show the distance distribution to TSS of 100,000 randomly selected positions. Tables at the top left in panels B, E and F report overlapping indexes and pairwise Wilcoxon test p-values between the distributions of lineage-specific sequence features and the random positions. Numbers on the right indicate the number of the respective sequence features.

Figure 5. Example intervals of the pan-genome assembly of *H. charithonia* (pink), *H. erato* (blue) and *H. melpomene* (orange) with alignment of lineage-specific genome sequences, transposable element (TE) annotations and ATAC-seq profiles in the pan-genome coordinate space. The plots show an illustrative interval of the pan-genome assembly near the gene *chiffon* (*chif*) and *sloppy paired 2* (*slp2*) that highlights sequences present in each of the genomes relative to the pan-genome (black shading underneath each of the graphs), lineage-specific sequences in each of the genomes (pink, blue and orange shading in graphs), TEs that overlap with lineage-specific sequences (dark red), and ATAC-seq profiles for head tissue (average of two biological replicates). Gray shading in the *H. charithonia* haplotype 2 (hap2) graph indicates an indel in the genome of a single *H. charithonia* individual. Red stars indicate ATAC-seq peaks with head-specific accessibility (compared to wing tissue) that intersect with a lineage-specific TE insertion. See Supplemental Fig. S7 for additional examples of intervals around *tropomodulin-1* (*tmod*) and *MICOS complex subunit Mic60* (*Mitofilin*). The Supplemental Material provides code to reproduce similar plots for any region in the pan genome.

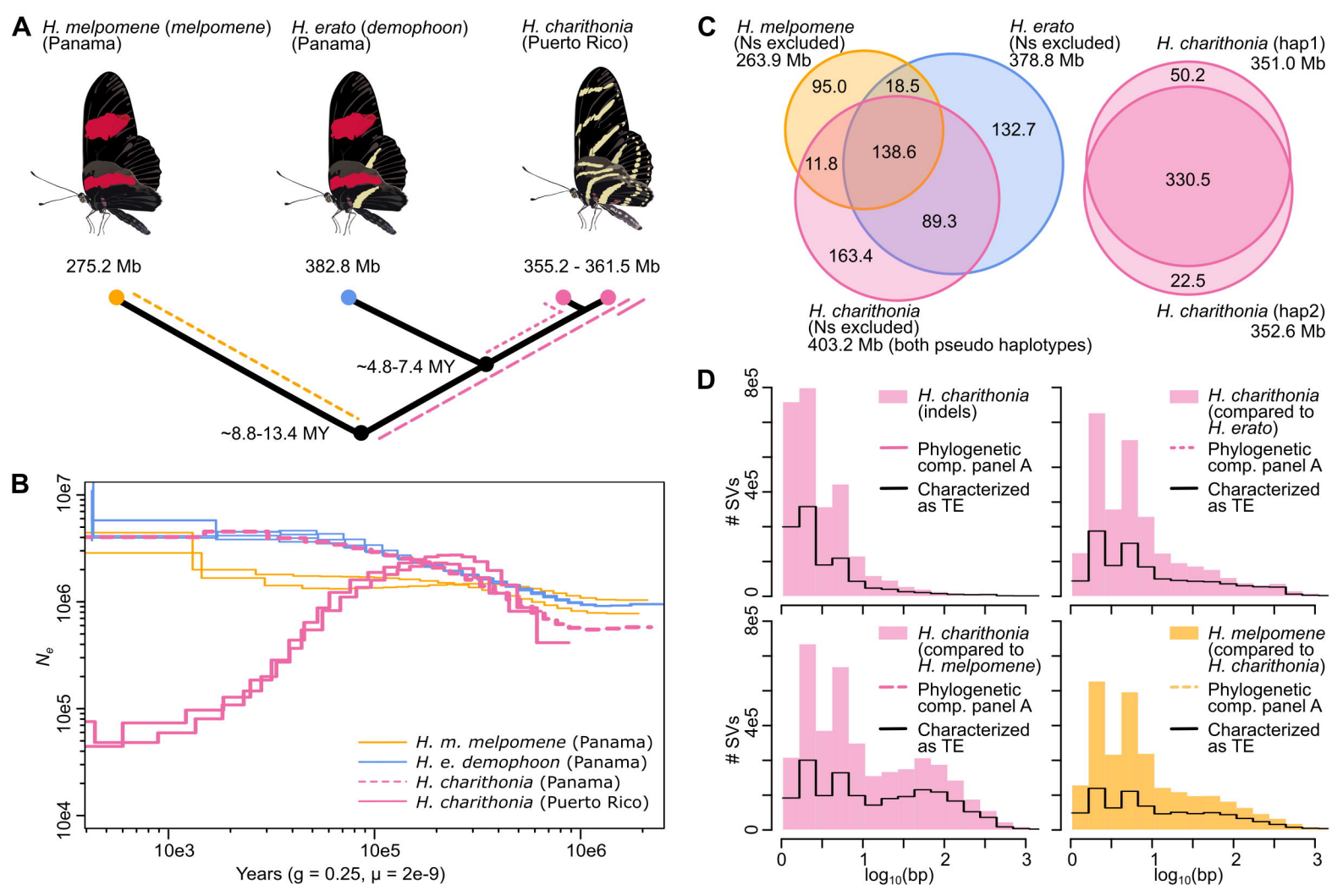
A
H. melpomene (melpomene)
(Panama)
H. erato (demophoon)
(Panama)
H. charithonia
(Puerto Rico)
275.2 Mb
382.8 Mb
355.2 - 361.5 Mb
~4.8-7.4 MY
~8.8-13.4 MY
B
10e7
10e6
10e5
10e4
Ne
10e3
10e5
10e6
Years (g = 0.25, μ = 2e-9)
H. m. melpomene (Panama)
H. e. demophoon (Panama)
H. charithonia (Panama)
H. charithonia (Puerto Rico)
C
H. melpomene
(Ns excluded)
263.9 Mb
H. erato
(Ns excluded)
378.8 Mb
H. charithonia (hap1)
351.0 Mb
95.0
18.5
132.7
11.8
138.6
89.3
163.4
50.2
330.5
22.5
H. charithonia
(Ns excluded)
403.2 Mb (both pseudo haplotypes)
H. charithonia (hap2)
352.6 Mb
D
8e5
4e5
0
SVs
H. charithonia
(indels)
Phylogenetic
comp. panel A
Characterized
as TE
H. charithonia
(compared to
H. erato)
H. charithonia
(compared to
H. melpomene)
H. melpomene
(compared to
H. charithonia)
0
1
2
3
log10(bp)

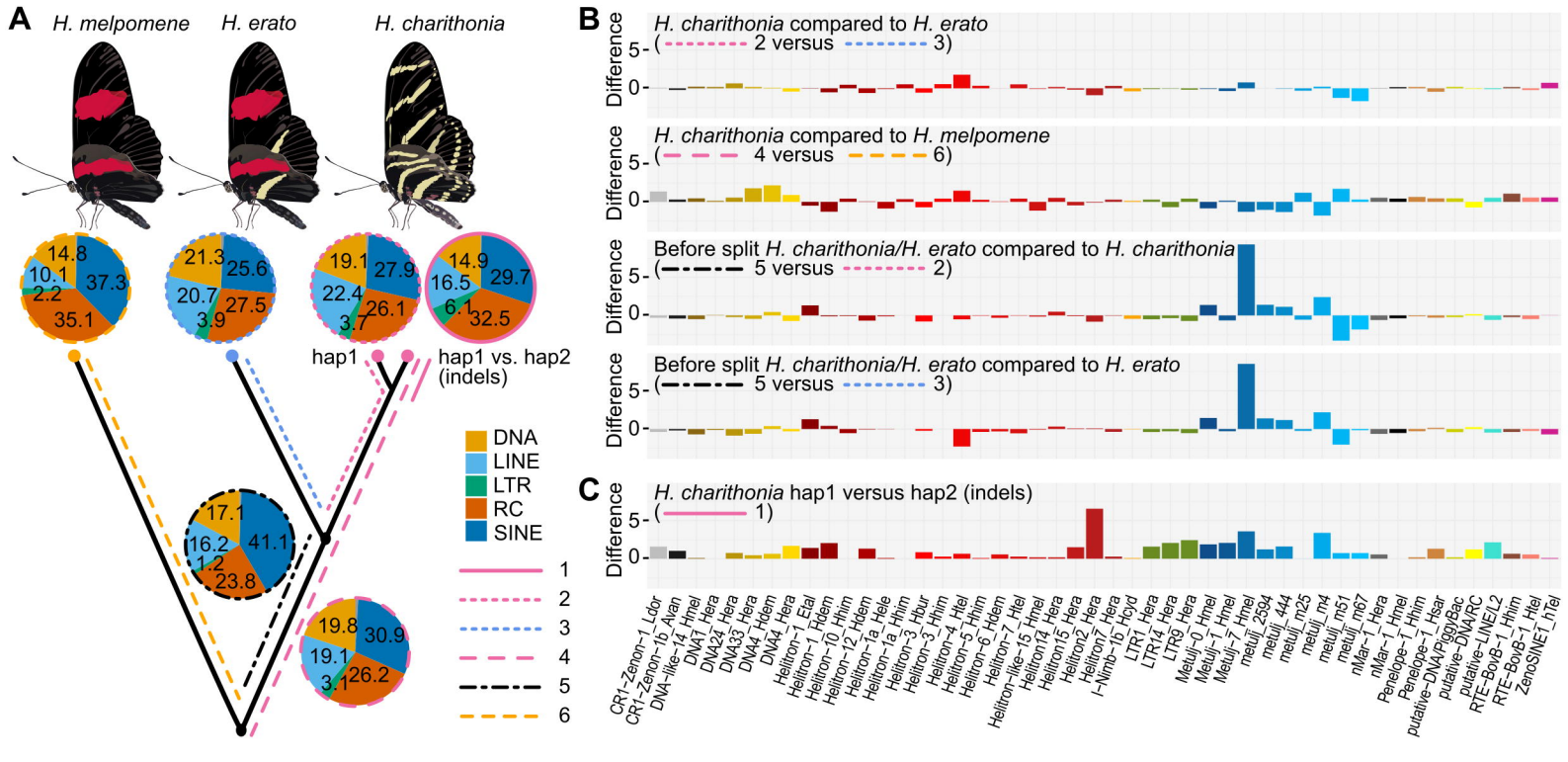
A
H. melpomene
H. erato
H. charithonia
14.8
10.1
2.2
37.3
35.1
21.3
25.6
20.7
27.5
3.9
19.1
27.9
22.4
26.1
3.7
14.9
29.7
16.5
6.1
32.5
hap1
hap1 vs. hap2 (indels)
17.1
16.2
41.1
1.2
23.8
19.8
30.9
19.1
26.2
3.1
DNA
LINE
LTR
RC
SINE
1
2
3
4
5
6
B
H. charithonia compared to H. erato
(2 versus 3)
H. charithonia compared to H. melpomene
(4 versus 6)
Before split H. charithonia/H. erato compared to H. charithonia
(5 versus 2)
Before split H. charithonia/H. erato compared to H. erato
(5 versus 3)
Difference
5
0
C
H. charithonia hap1 versus hap2 (indels)
(1)
CR1-Zenon-1_Ldor
CR1-Zenon-16_Avan
DNA-like-14_Hmel
DNA1_Hera
DNA24_Hera
DNA33_Hera
DNA4_Hdem
DNA4_Hera
Helitron-1_Etal
Helitron-1_Hdem
Helitron-10_Hhim
Helitron-12_Hdem
Helitron-1a_Hele
Helitron-1a_Hhim
Helitron-3_Hbur
Helitron-3_Hhim
Helitron-4_Htel
Helitron-5_Hhim
Helitron-6_Hdem
Helitron-7_Htel
Helitron-like-15_Hmel
Helitron14_Hera
Helitron15_Hera
Helitron2_Hera
Helitron7_Hera
I-Nimb-16_Hcyd
LTR1_Hera
LTR14_Hera
LTR9_Hera
Metulj-0_Hmel
Metulj-1_Hmel
Metulj-7_Hmel
metulj_2594
metulj_444
metulj_m25
metulj_m4
metulj_m51
metulj_m67
nMar-1_Hera
nMar-1_Hmel
Penelope-1_Hhim
Penelope-1_Hsar
putative-DNA/pggyBac
putative-DNA/RC
putative-LINE/L2
RTE-BovB-1_Hhim
RTE-BovB-1_Htel
ZenoSINE1_htel

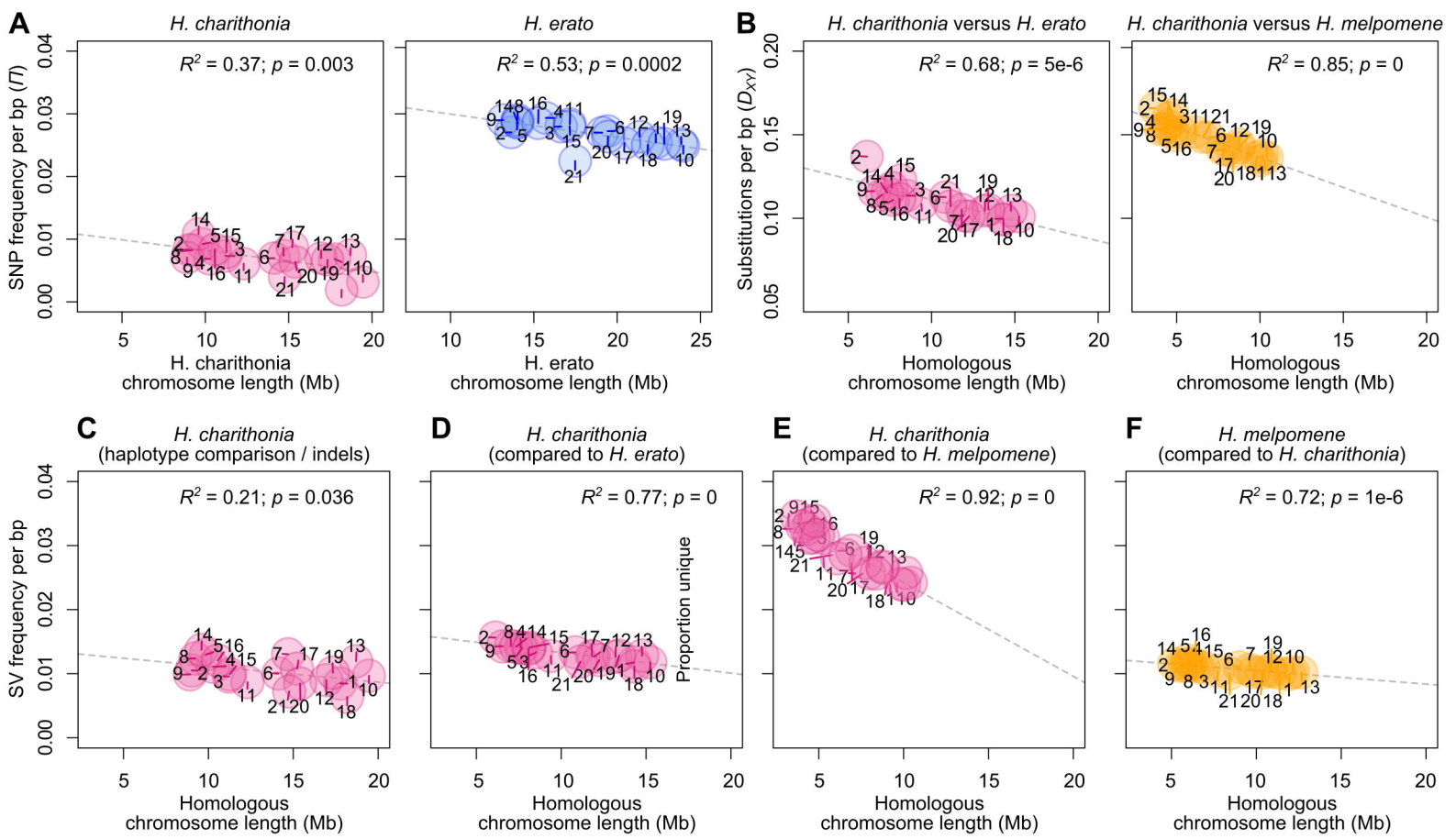
A
H. charithonia
H. erato
R^2 = 0.37; p = 0.003
R^2 = 0.53; p = 0.0002
SNP frequency per bp (Π)
H. charithonia chromosome length (Mb)
H. erato chromosome length (Mb)
B
H. charithonia versus H. erato
H. charithonia versus H. melpomene
R^2 = 0.68; p = 5e-6
R^2 = 0.85; p = 0
Substitutions per bp (D_{XY})
Homologous chromosome length (Mb)
C
H. charithonia
(haplotype comparison / indels)
R^2 = 0.21; p = 0.036
SV frequency per bp
D
H. charithonia
(compared to H. erato)
R^2 = 0.77; p = 0
Proportion unique
E
H. charithonia
(compared to H. melpomene)
R^2 = 0.92; p = 0
F
H. melpomene
(compared to H. charithonia)
R^2 = 0.72; p = 1e-6

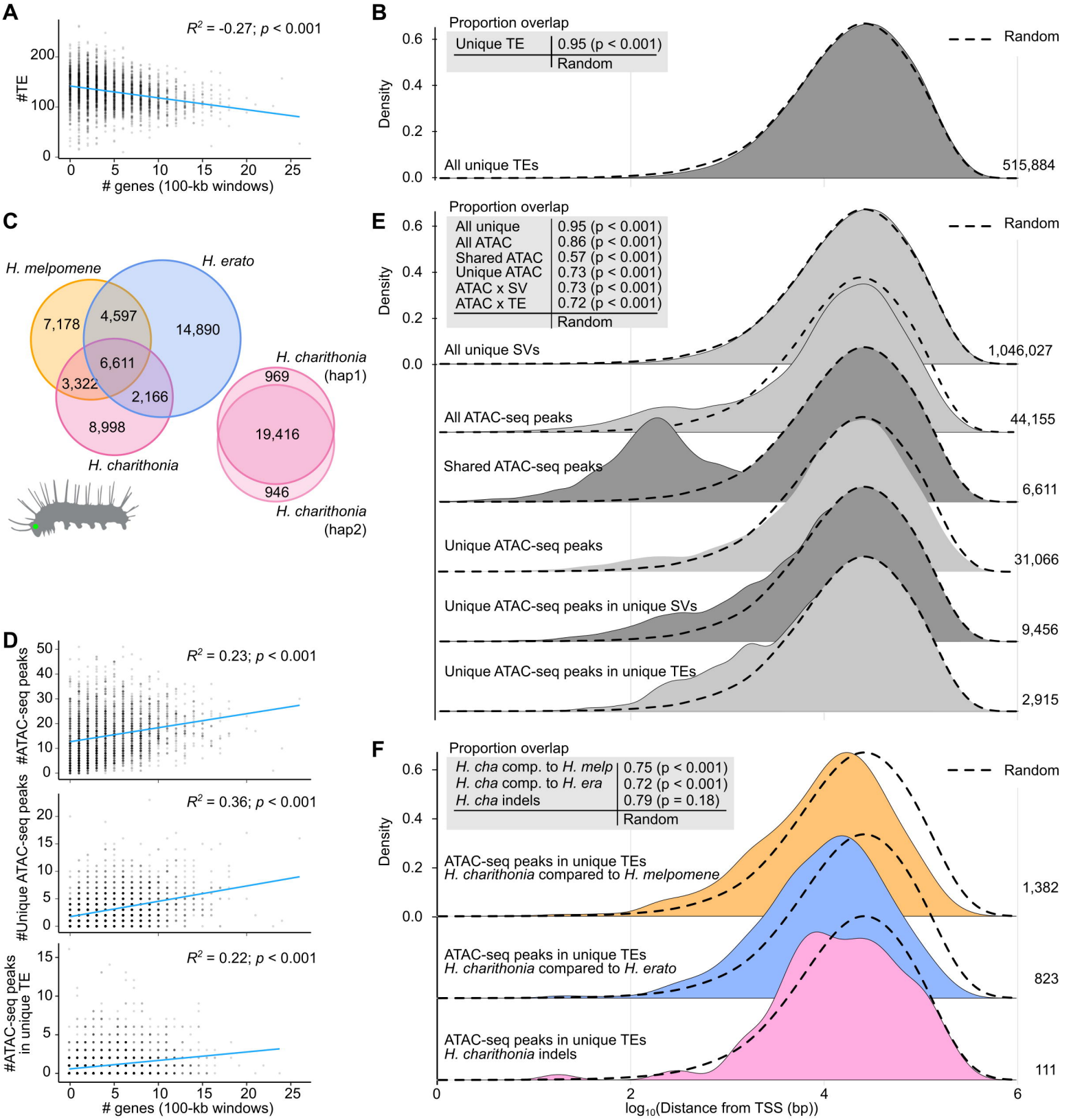
A
R^2 = -0.27; p < 0.001
#TE
genes (100-kb windows)
B
Proportion overlap
Unique TE | 0.95 (p < 0.001)
Random
Density
Random
All unique TEs
515,884
C
H. melpomene
H. erato
H. charithonia (hap1)
H. charithonia (hap2)
7,178
4,597
14,890
6,611
3,322
2,166
8,998
969
19,416
946
D
R^2 = 0.23; p < 0.001
#ATAC-seq peaks
R^2 = 0.36; p < 0.001
#Unique ATAC-seq peaks
R^2 = 0.22; p < 0.001
#ATAC-seq peaks in unique TE
genes (100-kb windows)
E
Proportion overlap
All unique | 0.95 (p < 0.001)
All ATAC | 0.86 (p < 0.001)
Shared ATAC | 0.57 (p < 0.001)
Unique ATAC | 0.73 (p < 0.001)
ATAC x SV | 0.73 (p < 0.001)
ATAC x TE | 0.72 (p < 0.001)
Random
Density
Random
All unique SVs
1,046,027
All ATAC-seq peaks
44,155
Shared ATAC-seq peaks
6,611
Unique ATAC-seq peaks
31,066
Unique ATAC-seq peaks in unique SVs
9,456
Unique ATAC-seq peaks in unique TEs
2,915
F
Proportion overlap
H. cha comp. to H. melp | 0.75 (p < 0.001)
H. cha comp. to H. era | 0.72 (p < 0.001)
H. cha indels | 0.79 (p = 0.18)
Random
Density
Random
ATAC-seq peaks in unique TEs
H. charithonia compared to H. melpomene
1,382
ATAC-seq peaks in unique TEs
H. charithonia compared to H. erato
823
ATAC-seq peaks in unique TEs
H. charithonia indels
111
log10(Distance from TSS (bp))

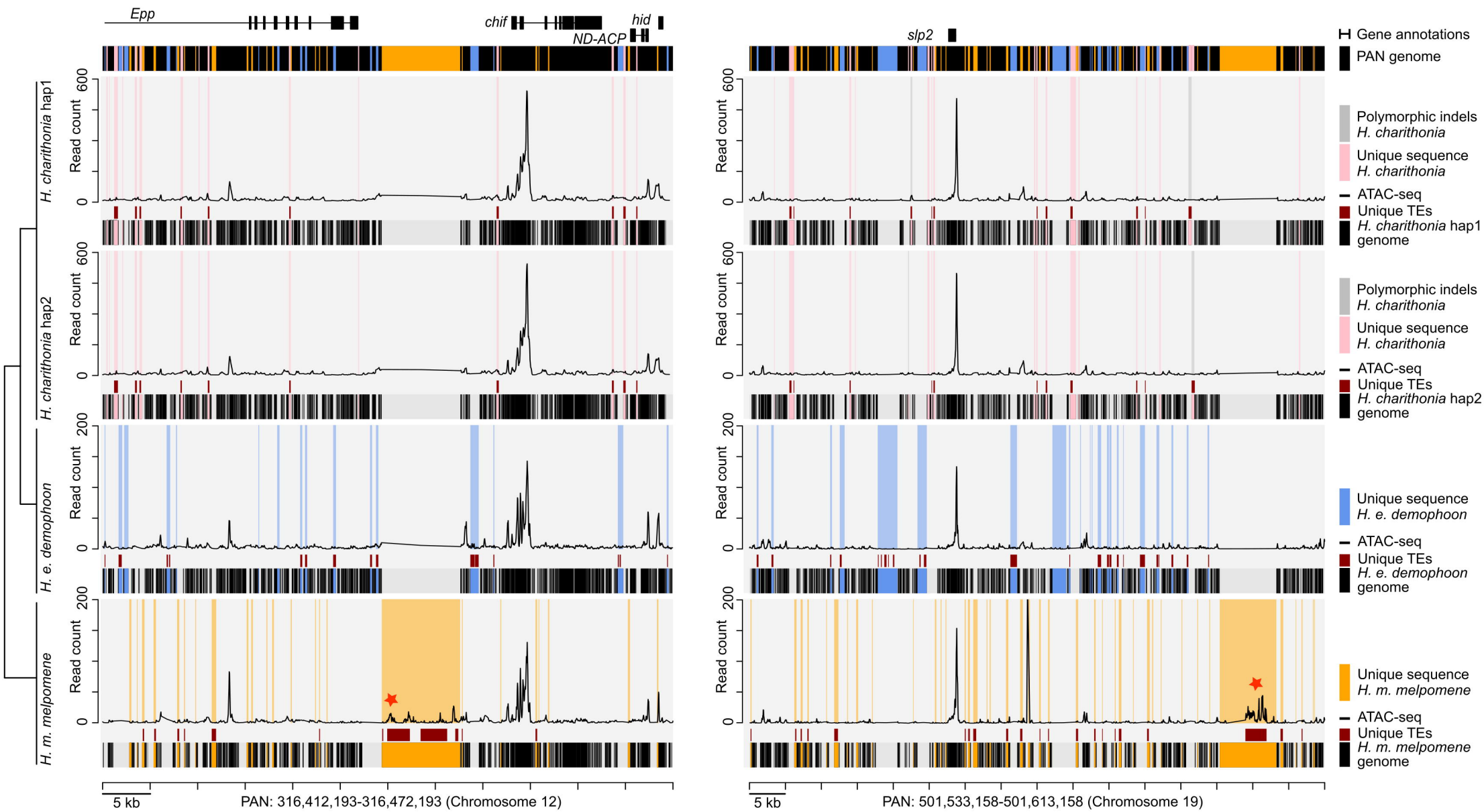
Epp
chif
hid
ND-ACP
slp2
Gene annotations
PAN genome
H. charithonia hap1
H. charithonia hap2
H. e. demophoon
H. m. melpomene
Read count
Polymorphic indels
H. charithonia
Unique sequence
H. charithonia
ATAC-seq
Unique TEs
H. charithonia hap1 genome
H. charithonia hap2 genome
Unique sequence
H. e. demophoon
H. e. demophoon genome
Unique sequence
H. m. melpomene
H. m. melpomene genome
5 kb
PAN: 316,412,193-316,472,193 (Chromosome 12)
PAN: 501,533,158-501,613,158 (Chromosome 19)

***Genome Research* 32:** 1862–1875

Erratum: A butterfly pan-genome reveals that a large amount of structural variation underlies the evolution of chromatin accessibility

Angelo A. Ruggieri, Luca Livraghi, James J. Lewis, Elizabeth Evans, Francesco Cicconardi, Laura Hebberecht, Yadira Ortiz-Ruiz, Stephen H. Montgomery, Alfredo Ghezzi, José Arcadio Rodriguez-Martinez, Chris D. Jiggins, W. Owen McMillan, Brian A. Counterman, Riccardo Papa, and Steven M. Van Belleghem

In the initial publication of the article mentioned above, one of the corresponding authors' email addresses was inadvertently omitted. The correct email addresses are as follows:

Corresponding authors: steven.vanbelleghem@kuleuven.be, rpapa.lab@gmail.com

In addition, the following corrections have been made to Figure 3: In part A, on the bottom *x*-axis labels, the terms "*H. charithonia*" and "*H. erato*" have been italicized. In part C, on the left *y*-axis label, the words "Proportion unique" have been removed; on the bottom *x*-axis label, the words "chromosome length (Mb)" have been clarified.

This article has already been corrected in both the PDF and full-text HTML files online.

doi: 10.1101/gr.277534.122

A butterfly pan-genome reveals that a large amount of structural variation underlies the evolution of chromatin accessibility

Angelo A. Ruggieri, Luca Livraghi, James J. Lewis, et al.

Genome Res. published online September 15, 2022
Access the most recent version at doi:10.1101/gr.276839.122